An ionic model for rhythmic activity in small clusters of embryonic chick ventricular cells

Trine Krogh-Madsen, Peter Schaffer, Anne D. Skriver, Louise Kold Taylor, Brigitte Pelzmann, Bernd Koidl and Michael R. Guevara

AJP - Heart 289:398-413, 2005. First published Feb 11, 2005; doi:10.1152/ajpheart.00683.2004

Am J Physiol Heart Circ Physiol 289: H398–H413, 2005.
First published February 11, 2005; doi:10.1152/ajpheart.00683.2004.

An ionic model for rhythmic activity in small clusters of embryonic chick ventricular cells

Trine Krogh-Madsen,[1,2] Peter Schaffer,[3] Anne D. Skriver,[1,2] Louise Kold Taylor,[1,2] Brigitte Pelzmann,[3] Bernd Koidl,[3] and Michael R. Guevara[1,2]

[1]*Department of Physiology and* [2]*Centre for Nonlinear Dynamics in Physiology and Medicine, McGill University, Montreal, Quebec, Canada; and* [3]*Center of Physiological Medicine, Institute of Biophysics, Medical University Graz, Graz, Austria*

Submitted 12 July 2004; accepted in final form 3 February 2005

Krogh-Madsen, Trine, Peter Schaffer, Anne D. Skriver, Louise Kold Taylor, Brigitte Pelzmann, Bernd Koidl, and Michael R. Guevara. An ionic model for rhythmic activity in small clusters of embryonic chick ventricular cells. *Am J Physiol Heart Circ Physiol* 289: H398–H413, 2005. First published February 11, 2005; doi:10.1152/ajpheart.00683.2004.—We recorded transmembrane potential in whole cell recording mode from small clusters (2–4 cells) of spontaneously beating 7-day embryonic chick ventricular cells after 1–3 days in culture and investigated effects of the blockers D-600, diltiazem, almokalant, and Ba^{2+}. Electrical activity in small clusters is very different from that in reaggregates of several hundred embryonic chick ventricular cells, e.g., TTX-sensitive fast upstrokes in reaggregates vs. TTX-insensitive slow upstrokes in small clusters (maximum upstroke velocity ~100 V/s vs. ~10 V/s). On the basis of our voltage- and current-clamp results and data from the literature, we formulated a Hodgkin-Huxley-type ionic model for the electrical activity in these small clusters. The model contains a Ca^{2+} current (I_{Ca}), three K^+ currents (I_{Ks}, I_{Kr}, and I_{K1}), a background current, and a seal-leak current. I_{Ca} generates the slow upstroke, whereas I_{Ks}, I_{Kr}, and I_{K1} contribute to repolarization. All the currents contribute to spontaneous diastolic depolarization, e.g., removal of the seal-leak current increases the interbeat interval from 392 to 535 ms. The model replicates the spontaneous activity in the clusters as well as the experimental results of application of blockers. Bifurcation analysis and simulations with the model predict that annihilation and single-pulse triggering should occur with partial block of I_{Ca}. Embryonic chick ventricular cells have been used as an experimental model to investigate various aspects of spontaneous beating of cardiac cells, e.g., mutual synchronization, regularity of beating, and spontaneous initiation and termination of reentrant rhythms; our model allows investigation of these topics through numerical simulation.

pacemaker; seal-leak current; rapid delayed rectifier potassium current block; slow inward calcium current block; bifurcation analysis

SPONTANEOUS ACTIVITY based on generation of the pacemaker potential (spontaneous phase 4, or diastolic, depolarization) is not normally found in adult ventricular muscle in situ, nor is it normally found in single cells freshly isolated from adult ventricular muscle. In contrast, early enough during development, ventricular muscle (or areas of the heart destined to eventually become ventricular muscle) can beat spontaneously (1, 97). Spontaneous electrical activity can also be seen in single cells and in small clusters of cells isolated from the embryonic chick ventricle (10, 17, 26, 49, 51, 78, 95), in the embryonic mouse ventricle (117), and in the neonatal rat ventricle (86).

After a couple of days in culture, the electrical activity in an isolated embryonic chick ventricular cell, in a small cluster of a few such cells, or in a sparse monolayer is very different from that in situ or in a reaggregate of hundreds or thousands of cells isolated from the ventricle. For example, when trypsin-dispersed ventricular cells from 7-day embryonic chick hearts are used, the upstroke velocity is much lower in single cells, in small clusters of cells, and in sparse monolayers (17, 49, 51, 95) than in reaggregates (14, 16, 19) or in the intact ventricle (19, 97, 98, 118). Spontaneous beating can be abolished by addition of tetrodotoxin (TTX), a blocker of the fast inward Na^+ current (I_{Na}), to the medium bathing reaggregates of trypsin-dispersed 7-day ventricular cells (16, 70), but spontaneous activity continues in single cells and monolayers (57, 70, 81, 95). However, spontaneous activity in some TTX-insensitive preparations can be abolished by addition of either of the Ca^{2+} channel blockers D-600 or diltiazem (49, 51).

We carried out an experimental study to characterize the electrical properties of spontaneously beating clusters of cells isolated from the 7-day embryonic chick ventricle and then assembled a mathematical model of this activity. The goal is to use this model to investigate phenomena seen in experiments, such as irregularity of beating in small clusters (10), mutual synchronization of pairs of cells (18), phase resetting and phase locking (9, 11, 52, 53), current-pulse-induced annihilation of spontaneous activity (90, 94), and spontaneous initiation and termination of spiral-wave reentrant motions in monolayers (6). Although ionic models of reaggregates of embryonic chick atrial cells have been described (9, 13, 52, 89, 90), we are not aware of any models of small clusters of isolated embryonic chick ventricular cells.

METHODS

Cell Isolation

Ventricular myocytes were isolated from embryonic chick hearts by means of techniques previously described (50) with modifications (79). The hearts of 7-day embryos were removed, and the ventricles were chopped off, minced, and transferred to flasks containing 0.25% trypsin (bovine pancreas; Boehringer Mannheim, Deisenhofen, Germany) in a nominally Ca^{2+}- and Mg^{2+}-free Hanks' balanced salt solution (HBSS; in mM: 137 NaCl, 5.4 KCl, 0.34 Na_2HPO_4, 0.44 KH_2PO_4, 4.2 $NaHCO_3$, and 5 glucose, pH 7.4). The flasks were placed in a shaker bath at 37°C for 7 min. The resulting cell suspension was gently agitated with a pipette and filtered through a 100-μm mesh. HBSS, supplemented with fetal calf serum (5% final

Address for reprint requests and other correspondence: M. R. Guevara, Dept. of Physiology, McGill University, 3655 Sir William Osler Promenade, Montreal, Quebec H3G 1Y6, Canada (E-mail: michael.guevara@mcgill.ca).

The costs of publication of this article were defrayed in part by the payment of page charges. The article must therefore be hereby marked "*advertisement*" in accordance with 18 U.S.C. Section 1734 solely to indicate this fact.

concentration), was added to stop trypsin activity. The cell suspension was centrifuged at ~100 *g* for 5 min at 4°C, the supernatant was discarded, and the cell pellet was resuspended in fresh trypsin-free HBSS. The centrifugation and resuspension processes were then repeated. The solution was centrifuged for a third time and resuspended in cell culture medium [M199 (Sigma) supplemented with 4% fetal calf serum, 2% horse serum, and 0.7 mM glutamine, pH 7.4] to yield a density of 5×10^5 cells/ml.

The cell suspension was separated into aliquots on nonadhesive plastic culture dishes that were incubated at 37°C in a water-saturated atmosphere of 95% air-5% CO_2. To obtain small clusters of cells, 0.6-ml aliquots of cell suspension were removed after 0.5–2 days and placed into the lumen of flexiPERM silicone rings (Heraeus, Hanau, Germany), which were attached to microscope slide coverslips. Coverslips with attached flexiPERM rings were placed in cell culture dishes (Greiner) and stored in the incubator. This procedure allowed the myocytes to adhere to the glass surface, where they could divide and form small clusters of cells. However, we can offer no guarantee that a particular cluster is made up entirely of cells that divided in culture.

Experiments were performed 2–36 h after the cells were plated, on clusters containing two to four cells. Recordings were made in the whole cell mode from clusters that were spontaneously beating before they were patched. We use clusters of a few cells, rather than single cells, because we were unable to obtain recordings of spontaneous activity from single cells. [It is also easier to successfully impale a cell in a cluster, rather than a single cell, if a conventional sharp microelectrode is used (17, 26).] In addition, the effect of the seal-leak current (I_{seal}; see below) on spontaneous activity is expected to be considerably smaller for a cluster than for a single cell (but see Ref. 78). For electrophysiological recording, the coverslip with attached myocytes was used to form the bottom of the experimental chamber, which was placed on the stage of an inverted microscope (Zeiss, Axiovert). The experimental chamber was perfused with extracellular solution (in mM: 137 NaCl, 5.4 KCl, 1.8 $CaCl_2$, 1.1 $MgCl_2$, 2.2 $NaHCO_3$, 0.4 NaH_2PO_4, 10 Na-HEPES, and 5.6 glucose, with pH adjusted to 7.4 with NaOH) at 36–37°C with a flow rate of 1.5 ml/min.

Electrophysiological Recording

The transmembrane potential (*V*) was recorded using the whole cell recording mode of the patch-clamp technique. Patch pipettes (~2 MΩ resistance) were pulled from glass capillary tubes and filled with pipette solution (in mM: 110 KCl, 4.3 K_2-ATP, 2 $MgCl_2$, 1 $CaCl_2$, 11 EGTA, and 10 K-HEPES, with pH adjusted to 7.4 with KOH) with estimated free Ca^{2+} concentration ($[Ca^{2+}] < 10^{-8}$ M. Electrode potentials were zeroed before seal formation. After the patch was broken, the transmembrane potential was recorded with an amplifier (model EPC-7, List, Darmstadt, Germany). The membrane capacitance was measured by integration of the capacitive transient in response to a voltage-clamp step from −50 to −60 mV. After capacity compensation, we compensated for series resistance by turning up the series-resistance compensation control (which controls the amount of positive feedback) to just below the value where ringing in the current monitor signal would occur. Usually, compensation could be made for >50% of series resistance. For generation of voltage-clamp protocols and for recording voltage and current, a personal computer equipped with pCLAMP version 5.5.7 software (Axon) and a DigiData 1200 interface (Axon) were used. Signals were also digitized at 44 kHz, pulse-code modulated, and stored on video cassette tape for offline analysis. The signal was played back, sampled at 1 kHz (Axotape, Axon Instruments), and stored on a disk file for computerized analysis.

Action Potential Parameters

Several parameters are measured to characterize spontaneous electrical activity. Interbeat interval (IBI) is the time between consecutive crossings of 0 mV on the upstroke of the action potential. The maximal diastolic potential (MDP) is the most negative voltage recorded during an action potential and the overshoot potential (OS) the most positive. The action potential amplitude (APA) is the difference between MDP and OS. Action potential duration (APD) is the time from the crossing of 0 mV on the upstroke to the time of 50% repolarization (APD_{50}) or 100% repolarization (APD_{100}). The diastolic depolarization rate (DDR) is the slope of the chord joining the point where (MDP + 1 mV) is crossed and the point 70 ms later (108, 114). The maximum rate of rise of the upstroke ($\dot{V}_{max}$) is computed using the greatest voltage difference between two consecutive samples on the upstroke (1-ms sampling interval).

Simulation Methods

Numerical integration of the Hodgkin-Huxley-type ionic model was carried out using a forward Euler scheme, with V at time $t + \Delta t$ calculated as follows

$$V(t + \Delta t) = V(t) - (\Delta t/C_m) \sum_i I_i(t)$$

where C_m is membrane capacitance and I_i represents the individual ionic currents described below. (A 4th-order Runge-Kutta integration scheme produced virtually superimposable results.) With our choice of time step ($\Delta t = 0.1$ ms), the change in voltage from time t to $t + \Delta t$ was kept to <1 mV. The value of each activation or inactivation variable (ξ_i) at time $t + \Delta t$ was obtained from its value at time t using the analytic formula

$$\xi_i(t + \Delta t) = \xi_i(\infty) - [\xi_i(\infty) - \xi_i(t)]e^{-\Delta t/\tau_i}$$

where $\xi_i(\infty)$ is the steady-state or asymptotic value of ξ_i at $V(t)$ and τ_i is the time constant of ξ_i at $V(t)$. L'Hôpital's rule was used to calculate α_n when V came to within ±0.1 mV of the value producing an indeterminate form. The numerical integration routine was written in C, and all variables were double precision (~16 significant decimal places).

Bifurcation analysis was carried out using AUTO, as incorporated in XPPAUT (25). The model equations file for use with XPPAUT is available as supplemental material (supplemental data for this article may be found at http://ajpheart.physiology.org/cgi/content/full/00683–4.2004.DC1).

Formulation of the Model

Our model consists of six currents: a slow inward Ca^{2+} current (I_{Ca}), a slow delayed K^+ current (I_{Ks}), a rapid delayed rectifier K^+ current (I_{Kr}), an inward rectifier K^+ current (I_{K1}), a linear time-independent background current (I_b), and a linear nonspecific seal-leak current (I_{seal}), generated by the leakage of ions through the gigaohm seal of the recording pipette. We now give the rationale for including each of these currents and for the particular formulation that we employ for each of these currents, as well as reasons for using a "first-generation," rather than a "second-generation," model.

Difficulties with second-generation models. In the earlier Hodgkin-Huxley-type ionic models of cardiac cells, all the concentrations of the various ionic species were held fixed, so that no provision had to be made for pumps and exchangers to regulate these concentrations. We refer to models that incorporate both of these refinements as second-generation models, in contrast to the earlier first-generation models. We formulate our model below as a more primitive first-generation model, because there are two major problems with the more physiologically realistic second-generation models: *1*) drift, with very slow long-term trends in some of the variables, particularly some ionic

concentrations (3, 21, 23, 24, 37, 45, 103, 116), and *2*) degeneracy, with nonuniqueness of equilibrium solutions such as steady states and limit cycles (23, 24, 30, 37, 102).

Drift has been managed in several ways: *1*) by finely adjusting parameters to achieve flux balance across the membrane (21), *2*) by adding an electroneutral Na^+ current of a precise size to produce stability of concentrations (74), *3*) by monitoring the stimulus current in a paced quiescent cell (37, 45), and *4*) by ensuring that certain ionic concentrations remain fixed (3, 55, 103, 121). It is not clear whether *strategies 1* and *2* are robust, because a change in some parameter in the model might require further fine adjustment of the stabilizing parameters. (This is reminiscent of a neutrally stable equilibrium.) *Strategy 3* is, of course, of no use in an unpaced pacemaker cell. *Strategy 4* defeats, at least in part, the initial intent in formulating the model as a second-generation model; e.g., when all the internal and external iconic concentrations are held constant, the Na^+-K^+ pump current (I_{NaK}) and the Na^+/Ca^{2+} exchange current (I_{NaCa}) are effectively background currents, and one is left essentially with a first-generation model, in which activity-dependent effects due to changes in certain ionic concentrations are not manifest.

The other major problem noted with second-generation models is degeneracy. In second-generation models of several different types of cardiac cells, the system of differential equations could be rewritten as a system of $N - 1$ equations in N unknowns (30, 102). The Jacobian is then singular, and there is a continuum of equilibrium points, rather than isolated equilibrium point(s), so that, e.g., the resting potential of a quiescent system depends on the initial conditions (30, 102). A similar finding of degeneracy holds for the limit cycle that corresponds to spontaneous activity (24, 30). It has been suggested that the original N-variable fully differential model should be recast as a differential-algebraic system, with the equation controlling voltage being algebraic and the remaining $(N - 1)$ equations being differential (23, 24, 30, 37, 45, 102). In one report in a sinoatrial (SA) node model in which the differential-algebraic formulation was used, it was stated that there was no long-term drift (23). In earlier work in which drift was abolished by making some ionic concentrations fixed, this also had the unintended benefit of removing the degeneracy, thus allowing the bifurcation analysis of isolated equilibria by means of continuation techniques (103; see also Refs. 55 and 121).

Finally, in situations such as ours in which cells are studied using patch micropipettes, a more realistic model of the experimental situation is one in which internal concentrations are kept fixed as a result of Ca^{2+} buffering with EGTA and dialysis of the cell contents of a very small cell volume against the much larger pipette volume (55, 121). Making concentrations fixed then also removes degeneracy and drift. Given all the above uncertainties and complications and given that very little information is available about the control of intracellular ionic concentrations in our cells, we decided to use a first-generation model, as have some authors of other quite recent studies (3).

Capacitance. Unless stated otherwise, ventricular and atrial cells will refer to embryonic chick ventricular and atrial cells, respectively, and *n*-day will refer to a cell isolated from the embryo after *n* days of incubation. Because the capacitance of a single 7-day ventricular cell in our laboratory is 8–9 pF, we set the capacitance in our three-cell model cluster to 25.5 pF. Our value of the single-cell capacitance agrees with that reported in several whole cell voltage-clamp studies employing single 7-day ventricular cells [e.g., 5–10 pF (29) and 4–7 pF (44)]. We model the cluster, which is a mutually synchronized population oscillator, as an isopotential preparation (27).

I_{Ca}. I_{Ca} has been described in 7-day reaggregates of ventricular cells (72), in small clusters of ventricular cells (28, 79), in single ventricular cells (13, 28, 42, 44), and at the single-channel level (43, 68). In one laboratory, L-type I_{Ca} ($I_{Ca,L}$) was found in 11 of 12 6-day ventricular cells, and T-type I_{Ca} ($I_{Ca,T}$) was found in the remaining cell (13). In another laboratory, only $I_{Ca,L}$ was found in 7-day ventricular cells (68). In a third study, both currents were found, but in only 45% of 7-day ventricular cells was I_{Ca} clearly separable into $I_{Ca,L}$ and $I_{Ca,T}$ on the basis of the voltage threshold for activation (44). In these cells, $I_{Ca,T}$ is half-inactivated at -49 mV, whereas $I_{Ca,L}$ is half-inactivated at -27.5 mV. In the 55% of cells with nonseparable I_{Ca}, half-inactivation occurs at -42.8 mV.

We have chosen to use a nonseparable description of I_{Ca} in our model

$$I_{Ca} = g_{Ca} df (V - E_{Ca})$$

where g_{Ca} is the maximal conductance, d is the activation variable, f is the inactivation variable, and E_{Ca} is the reversal potential, which we set to 40 mV on the basis of our own voltage-clamp results (79). The equations governing d and f are given in the APPENDIX.

The steady-state inactivation (f_∞) curve of the nonseparable current in 7-day ventricular cells, which lies between the inactivation curves for $I_{Ca,L}$ and $I_{Ca,T}$, is taken from Fig. 9 of Ref. 44. Because the steady-state activation (d_∞) curve of the nonseparable current was not reported, we assume that it lies between the $I_{Ca,L}$ and $I_{Ca,T}$ activation curves of Fig. 10 of Ref. 44 and that it has an intermediate slope factor. We have chosen the values of parameters so that the d_∞ curve is closer to the $I_{Ca,L}$ than to the $I_{Ca,T}$ activation curve, in order that the peak-current current-voltage (*I-V*) curve has a maximum at ~0 mV, which is close to the experimental value for the nonseparable current (44). Figure 1*A* shows the steady-state d_∞ and f_∞ curves.

There are no systematic reports of the time constants of activation (τ_d) and inactivation (τ_f) of the nonseparable current. We therefore take the expressions unchanged from Ref. 66, which describes $I_{Ca,L}$ in a 37°C guinea pig model. The τ_d curve (Fig. 1*B*) has a typical bell shape, whereas the τ_f curve (Fig. 1*B*) has the U shape that is seen in mammalian cells and in 7-day ventricular reaggregates (72).

We have set g_{Ca} so that $\dot{V}_{max}$ is 9.5 V/s in the model, which is close to our mean experimental result (8.5 V/s). The peak-current *I-V* curve then has a maximum value of ~30 pA/pF at ~0 mV (Fig. 1*C*), which is within the range seen in our cells [79; see also Fig. 4*C* of Ref. 44 and Fig. 1 of Ref. 13, scaled for differences in capacitance and

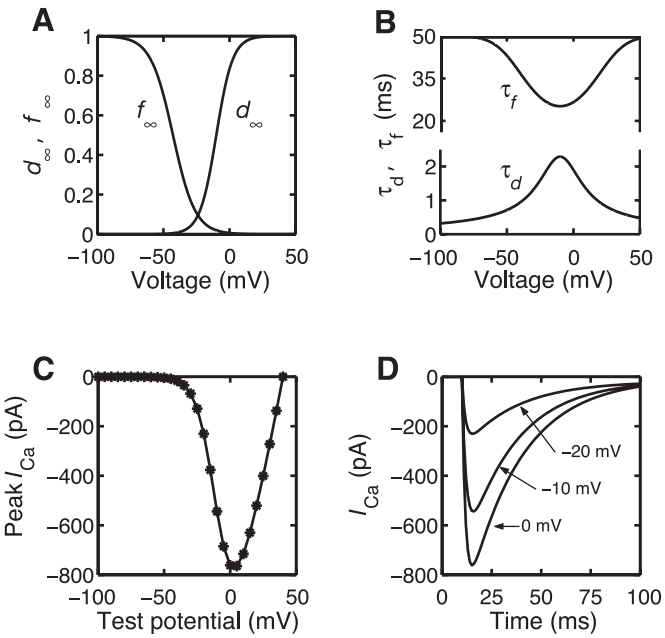

Fig. 1. Characteristics of slow inward Ca^{2+} current (I_{Ca}) in the model. *A*: steady-state activation (d_∞) and inactivation (f_∞) curves. *B*: time constants of activation (τ_d) and inactivation (τ_f). *C*: peak I_{Ca} in voltage-clamp steps from a holding potential of −80 mV to various test potentials (protocol of Ref. 44). *D*: simulated current during voltage-clamp steps from a holding potential of −80 mV to 0, −10, and −20 mV (protocol of Ref. 44).

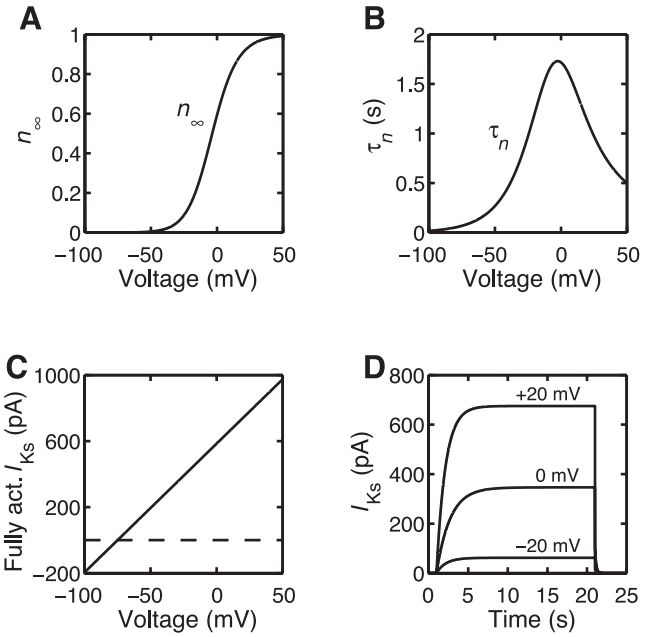

Fig. 2. Characteristics of slow delayed K^+ current (I_{Ks}) in the model. *A*: steady-state activation (n_∞) curve. *B*: time constant of activation (τ_n). *C*: fully activated (act) I_{Ks}. *D*: simulated current during voltage-clamp steps from a holding potential of −60 mV to −20, 0, and +20 mV (protocol of Ref. 8).

temperature ($Q_{10} \cong 3$ for peak current amplitude for guinea pig ventricular cells (7))]. Figure 1*D* shows that the current traces from a voltage-clamp protocol in the model are similar, in magnitude and time course, to the corresponding experimental traces in Ref. 79 (see also Fig. 7*B* of Ref. 44, scaled for temperature and capacitance).

Because internal Ca^{2+} is buffered by our pipette solution, we do not include Ca^{2+}-dependent inactivation of I_{Ca} (13) in our description; instead, we use only voltage-dependent inactivation to reproduce the time course of the inactivation process that is seen experimentally (44). Nor do we include the two time constants of inactivation seen in 7-day ventricular reaggregates (72).

Delayed K^+ currents. The delayed K^+ currents I_{Ks} and I_{Kr} have been described in reaggregates of ventricular cells (13, 14, 88) and atrial cells (9, 88, 89), in small clusters of ventricular cells (79), and in single ventricular (8) and atrial (12) cells. These currents have also been observed at the single-channel level in ventricular cells (8, 67).

Two components of the delayed current, initially termed I_{x1} and I_{x2}, have been seen in atrial reaggregates (89). These two currents correspond to those more recently termed I_{Kr} and I_{Ks}, respectively, in isolated adult mammalian ventricular cells. I_{x2}, or I_{Ks}, has been described in 7-day ventricular reaggregates (14, 15), in single ventricular cells (8), and in small clusters of such cells (79). However, although I_{x1} is robust in experiments carried out using sharp microelectrodes on atrial (89) and ventricular (13) reaggregates, it has not been seen in whole cell clamp experiments carried out using patch pipettes on isolated 7- to 10-day ventricular cells (8) or on single 6- to 11-day atrial cells or small clusters of such cells (12). This might be due to an intrinsic absence of the current [e.g., there is good evidence for cell-cell contact-dependent regulation of expression of two different K^+ channels in cultured adult rat ventricular cells (35)] or to rapid washout of this current in the whole cell ruptured-patch recording mode. Indeed, it has been suggested that the main difference in the action potentials of atrial reaggregates and small clusters of atrial cells can be accounted for by the absence of I_{x1} in the latter (see Fig. 9 of Ref. 12 and Fig. 17 of Ref. 13). In contrast to the above-mentioned reports, in our 7-day ventricular clusters, the envelope-of-tails test shows two components (79), and application of the specific I_{Kr} blocker almokalant (113) removes the more rapidly deactivating component of the tail current. In addition, almokalant produces changes in the action potential consistent with I_{Kr} block (see below). At the single-channel level, a K^+ channel that activates over a voltage range similar to that over which I_{Kr} activates has been described (8). We thus incorporate the I_{Ks} and I_{Kr} components into our model.

For I_{Ks}, we use the formulation previously used in an atrial reaggregate model (52)

$$I_{Ks} = g_{Ks} n (V - E_{Ks})$$

where n is the activation variable. We set the reversal potential (E_{Ks}) equal to −75 mV, the value found in our cells (79; see also Fig. 1*C* of Ref. 8). This value is depolarized to the equilibrium potential for K^+ of −85 mV, computed from the Nernst equation at 37°C, external [K^+] of 5.4 mM, and pipette [K^+] of 129 mM. This relatively depolarized value of E_{Ks} has been found in many studies on I_{Ks} and has been attributed to a slight permeability of the channel to Na^+ (65, 121). In obtaining the formulas for the rate constants α_n and β_n (see APPENDIX), we have first divided the original equations (52) by a factor of 3, to obtain a τ_n curve consistent with the experimental values in single ventricular cells at room temperature (see Fig. 2*C* of Ref. 8), and then multiplied α_n and β_n by a factor of 2, in correspondence with the reported Q_{10} (111), to obtain values appropriate for our experimental temperature of 36–37°C (Fig. 2*B*). The maximal conductance (g_{Ks}) was set to give a fully activated *I-V* curve (Fig. 2*C*), similar to that seen experimentally (see Fig. 1*C* of Ref. 8), scaled for capacitance and temperature ($Q_{10} \cong 2$) (111). The steady-state activation curve (Fig. 2*A*) and the voltage-clamp currents (Fig. 2*D*) are similar to those previously reported from our laboratory at 37°C (79), as well as those reported elsewhere (8), when compensated for temperature.

For I_{Kr}, we use the formulation

$$I_{Kr} = g_{Kr} s z(V) (V - E_{Kr})$$

where s is the activation variable, and we introduce $z(V)$ to provide inward rectification so that the fully activated *I-V* relation (Fig. 3*C*) is similar in shape to that seen in atrial reaggregates (see Fig. 8*C* of Ref.

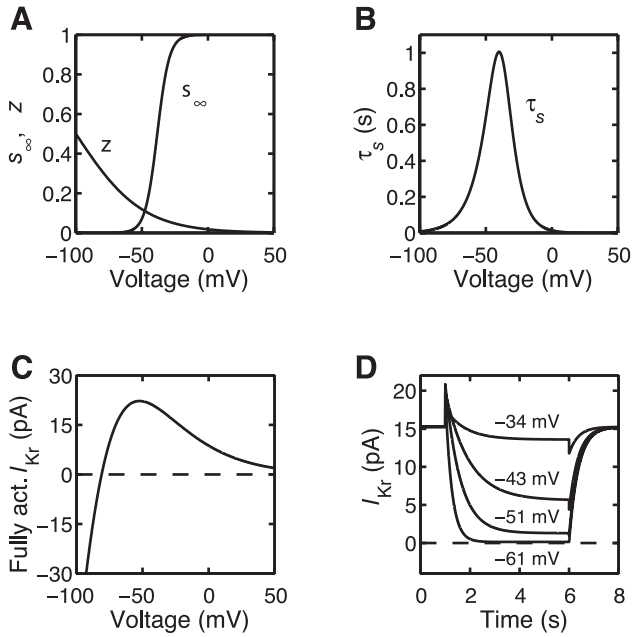

Fig. 3. Characteristics of rapid delayed rectifier K^+ current (I_{Kr}) in the model. *A*: steady-state activation (s_∞) curve and rectification variable (z). *B*: time constant of activation (τ_s). *C*: fully activated I_{Kr}; note pronounced rectification. *D*: simulated current during voltage-clamp steps from a holding potential of −26 mV to −34, −43, −51, and −61 mV (protocol of Ref. 89).

89). Our form of $z(V)$ (see APPENDIX; Fig. 3*A*) gives more current at depolarized voltages than the fit originally used in Fig. 8*C* of Ref. 89, which corresponds to the fact that we observe a maintained almokalant-sensitive current at positive voltages (see RESULTS). The function $z(V)$ represents the very rapid inactivation described for the human ether-a-go-go-related gene (HERG) subunit of I_{Kr} (92, 93) and for I_{Kr} in single SA node cells (54, 76). The reversal potential (E_{Kr}) was set to −81 mV on the basis of observations in our laboratory. (This closeness of E_{Kr} to the Nernst potential of −85 mV for K^+ is characteristic of I_{Kr} in many other cardiac preparations.) Our setting of the maximal conductance (g_{Kr}) yields a maximum value of the fully activated current (Fig. 3*C*) comparable to that seen in atrial reaggregates (89).

The gating variable s is governed by equations (see APPENDIX) slightly modified from those in Table I of Ref. 89, so as to fit more closely the data points in Fig. 5, *A* and *B*, of Ref. 89 (the original equations in Table I do not give the fitted curves shown in Fig. 5, *A* and *B*). With these modifications, our s_∞ and τ_s curves (Fig. 3, *A* and *B*) are very close to the data in Fig. 5, *A* and *B*, of Ref. 89. A voltage-clamp protocol (Fig. 3*D*) gives currents similar to those in Fig. 4 of Ref. 89. We use only one time constant of activation; in SA node cells, two time constants of activation of I_{Kr} have been described (76).

I_{K1}. *I-V* curves of reaggregates of 7-day ventricular cells (14, 15), in small clusters of 7-day ventricular cells (79), and in single 7-day ventricular cells (4) show marked inward rectification at very negative potentials because of the presence of I_{K1}. There is also evidence for this current at the single-channel level in 7-day ventricular cells (67). We have thus included an I_{K1} component in our model (Fig. 4), taking the formulation from a guinea pig ventricular cell model (65)

$$I_{K1} = g_{K1}K1(V - E_{K1})$$

where we set $E_{K1} = -81$ mV, which is, as commonly observed, slightly depolarized to the calculated Nernst potential for K^+ (−85 mV). Although a time-independent description of I_{K1} (i.e., $K1 = K1_\infty$) was originally used (65), we employ the time-dependent description to allow us to later formulate a model with stochastic gating kinetics to investigate beat-to-beat fluctuations in IBI (unpublished observations). However, the time constant of this current is so small ($\tau_{K1} <$ 0.2 ms over the operative range of voltage; Fig. 4*B*) that the current is virtually identical in the time-dependent and time-independent descriptions. The maximal conductance (g_{K1}) is reduced from the guinea pig value to reflect the smaller I_{K1} earlier in development (15, 41). The steady-state *I-V* curve for the total current (see curve in Fig. 7*A*) is then very flat between −70 and −30 mV, which agrees with our experimental results (see symbols in Fig. 7*A*). The I_{K1} *I-V* curve (see Fig. 7*C*) is the main contributor to the positive slope of the total-current *I-V* curve at very hyperpolarized potentials (see Fig. 7*A*) and is similar to the Ba^{2+}-sensitive current at hyperpolarized potentials (4, 79).

I_b. In addition to I_{K1}, which is outward at potentials depolarized to −81 mV, there is inward background current in 7-day ventricular reaggregates (14). This component has been modeled as a Na^+ current

$$I_b = g_b(V - E_b)$$

where $E_b = 40$ mV and g_b is obtained from Fig. 11 of Ref. 14, scaled for capacitance. Figure 7*D* gives the *I-V* relation for this linear current.

I_{seal}. It has been pointed out that I_{seal} flowing through the pipette gigaohm seal can be appreciable with respect to the total current flowing during diastolic depolarization for a very small cell with a high input resistance (20). We therefore add a nonspecific I_{seal} in our model

$$I_{seal} = g_{seal}(V - E_{seal})$$

with g_{seal} corresponding to a nominal seal-leak resistance of 5 GΩ (20) and $E_{seal} = 0$ mV. Figure 7*D* gives the *I-V* relation of I_{seal}.

Currents Not Included in the Ionic Model

I_{Na}. There is voltage-clamp evidence for the existence of I_{Na} in reaggregates of 7- to 11-day ventricular cells (22, 72), in single 2- to 18-day ventricular cells (29, 40, 82, 83, 112), and at the single-channel level in 7-day ventricular cells (64, 112). Voltage-clamp studies of 7-day ventricular clusters in our laboratory show a fast inward current upon a depolarizing clamp step from potentials more hyperpolarized than about −60 mV. However, our clusters have a very low upstroke velocity (8.5 V/s), suggesting that I_{Na} might not contribute appreciably to the upstroke phase, especially because Ca^{2+} channel blockers abolish spontaneous activity (see Fig. 9, *A* and *B*). The MDP (−60 mV in the clusters and −67 mV in the model) is sufficiently depolarized to essentially render I_{Na} fully inactivated, because the foot of the I_{Na} steady-state inactivation curve lies at about −50 to −60 mV in 7-day ventricular reaggregates (22) and 7-day ventricular cells (29, 82). Indeed, addition of I_{Na} to our model, on the basis of the conductance and the activation and inactivation curves from single 7-day ventricular cells (29) and the time constants from 11-day reaggregates (22), slightly increases $\dot{V}_{max}$ from 9.5 to 10.2 V/s. In contrast, reaggregates of trypsin-dissociated 7-day ventricular cells have a TTX-sensitive upstroke velocity of 120 V/s in 1.3 mM K^+ and 91 V/s in 4.5 mM K^+, presumably due to the more hyperpolarized MDP of about −90 and −76 mV, respectively (16, 19).

I_{Na} can also be involved in generating the pacemaker potential. There is indeed evidence that I_{Na} is necessary in some isolated embryonic cells for the generation of spontaneous activity. After 24 h in culture, 37% of single cells dissociated using trypsin from 7-day hearts (whole hearts, atria, or ventricles) stop beating after the addition of 10^{-5} g/ml TTX (70), showing that I_{Na} is crucial in generating spontaneous activity in these cells. However, the percentage of TTX-insensitive cells increases with time spent in culture: 43% at 4 h, 64% at 24 h, and 100% at 48 h (57). In contrast, reaggregates of trypsin-dissociated 7-day ventricular cells that are cultured for 24–72 h stop beating when exposed to TTX (16, 70). This difference in the response to TTX almost certainly indicates the importance of cell-to-cell interactions (19, 69). In newborn rabbit SA node, a TTX-sensitive current, which gradually disappears within the first 30 days postnatum, has been implicated in the generation of diastolic depolarization (2). This contribution is not due to the I_{Na} window current but, rather, is a consequence of relatively slow inactivation of I_{Na} in the pacemaker range of potentials. Recently, modeling work has suggested a role for a persistent component of a mutated I_{Na} in the generation of diastolic depolarization in long Q-T (LQT3) syndrome (105).

A third role for I_{Na} is maintenance of the plateau of the action potential, e.g., via a window current contribution. Application of TTX results in a shortening of the APD in some 7-day ventricular cells before they stop beating (64). Single Na^+ channels occasionally (1 of 100 beats) stay open throughout the action potential plateau (64) and burst for >150 ms in 16% of trials during a long voltage-clamp step (40). Because these long openings do not persist into diastole (see Fig. 1 of Ref. 64), they would not contribute to diastolic depolarization. Incorporation of our standard Hodgkin-Huxley-type I_{Na} into the

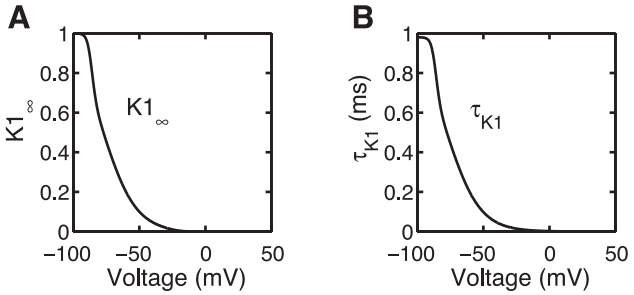

Fig. 4. Characteristics of inward rectifier K^+ current (I_{K1}) in the model. *A*: steady-state activation ($K1_\infty$) curve. *B*: time constant of activation (τ_{K1}).

model, as described above, results in a slight 3-ms increase in APD_{50} and a slight 5-ms increase in APD_{100}.

Pacemaker current. The pacemaker current (I_f) has been reported in ventricular reaggregates (4, 14, 15, 87, 88) as well as in single atrial and ventricular cells and small clusters of such cells (4, 5, 85). The midpoint of the activation range of I_f is ~30 mV more negative in single ventricular cells and small clusters than in reaggregates, with the foot of the activation curve of this hyperpolarization-activated current lying at −70 mV in single cells and small clusters (5). In our clusters, we find I_f activated at potentials negative to −70 mV (79). On the basis of the conductance, reversal potential, kinetics, and activation curve described in Ref. 5, we find that addition of I_f to the model causes only a very slight decrease in IBI from 392 to 390 ms. The MDP in our cells is, hence, too depolarized for I_f to activate and contribute significantly to pacemaking activity; therefore, we do not include it in our model.

Transient outward current. Although the size of the transient outward current (I_{to}) increases with development, the number of isolated ventricular cells possessing I_{to} is extremely low: 7 of ~300 cells at 3 days, 5 of ~200 cells at 10 days, and 5 of ~100 cells at 17 days (84). At the single-channel level, an early outward channel appeared in only 1 of 80 patches from 7-day ventricular cells (67). I_{to} was not seen in single atrial cells (12), nor was it "clearly observed" in 7- to 12-day atrial reaggregates (9). Moreover, in our own voltage-clamp experiments, we have also found no evidence of I_{to} in the clusters. In the SA node, the I_{to} density is smaller in cells with a smaller capacitance (58, 109). For these reasons, we do not include I_{to} in our model.

Cl^- current. A time-independent Cl^--sensitive current (I_{Cl}) has been described in isolated 11-day ventricular cells (63). We do not include I_{Cl} explicitly in the model, but we consider it to be a component of I_b.

I_{NaK} and I_{NaCa}. Currents provided by ion pumps and exchangers, e.g., I_{NaK}, I_{NaCa}, and the Ca^{2+} pump, also contribute to V. We employ a first-generation model, which does not have an Na^+-K^+ pump, an Na^+/Ca^{2+} exchanger, a Ca^{2+} pump, internal Ca^{2+} dynamics, and variable ionic concentrations. However, I_{NaK} and I_{NaCa} are present in 7-day ventricular cells. Although these currents are included in several recent ionic models of cardiac tissue, we do not include them in our model, because this would result in a second-generation model.

In our laboratory, 10 μM ouabain has been used to block I_{NaK} in 7- to 10-day ventricular cells or in small clusters of such cells (48). After 1 min of superfusion, the IBI first decreases, due to an increase in DDR, OS and MDP gradually fall, APD rises, and IBI increases, so that within a few minutes, spontaneous activity ceases, with the membrane coming to rest at about −30 mV. (Sharp microelectrodes were used in these experiments, so that artifact due to dialysis and current rundown was minimal.) A similar result is seen in 11-day cells cultured as a confluent layer or polystrand, except the initial effect is seen immediately, presumably because of the use of a perfusion system with rapid perfusate changeover (half-time of ~5 s), with the membrane coming to rest at about −40 mV (see Fig. 1 of Ref. 39). It has been estimated that I_{NaK} contributes 0.35 pA/pF at −70 mV in spontaneously beating 11-day reaggregates (100). In another report on 11-day reaggregates at an internal $[Na^+]$ of 41 mM, the ouabain-sensitive current amounts to 1.7 pA/pF and is independent of voltage over the operating range effective in our clusters (from −60 to +20 mV) (see Fig. 1 of Ref. 99). This value scales to ~0.5 pA/pF at an internal $[Na^+]$ of 10 mM (see Fig. 7 of Ref. 99), which agrees with SA node modeling work (54).

In our model, we can thus mimic the effect of blocking the electrogenic component of I_{NaK} by adding a constant depolarizing current of 10.2 pA (i.e., 0.4 pA/pF). This has the effect of decreasing IBI from 392 to 337 ms and depolarizing the MDP from −67 to −61 mV; both effects are seen immediately upon block of I_{NaK} in an experiment (see Fig. 1*B* of Ref. 39). Because the electrogenic component of I_{NaK} is removed within a few seconds of the start of block (Fig. 1 of Ref. 100), some secondary change must be responsible for the cessation of activity that occurs some minutes later (see Fig. 1 of Ref. 39). The most likely candidates are the rises in internal $[Na^+]$ and $[Ca^{2+}]$ after I_{NaK} block, which occur with a time course on the order of minutes (38, 39).

There is clear evidence for I_{NaCa} in 11-day ventricular reaggregates (100) and 11-day cells cultured as a confluent layer or polystrand (38). The maximum amplitude of I_{NaCa} in embryonic chick cells is about the same as in guinea pig ventricular cells (62). However, because of the difficulties inherent in interpreting experiments attempting to characterize I_{NaCa}, many of its fundamental properties (e.g., stoichiometry) remain uncertain in embryonic chick ventricular cells (62). The extent to which I_{NaCa} is involved in generating diastolic depolarization in SA node cells is controversial (56) and is very different in different SA node models, to the extent that although I_{NaCa} is inward in most models, it is outward in at least one (see Fig. 7 of Ref. 54). In addition, in a model of spontaneous activity induced by suppression of I_{K1} in guinea pig ventricular cells, I_{NaCa} is inward during the pacemaker potential (91). We are not aware of any studies of the Ca^{2+} pump in embryonic chick ventricular cells.

Given the above problems, as well as other problems described earlier involving degeneracy and drift in models where pumps and exchangers have been added, we have chosen not to include these currents in our model. Rather, I_{NaK} can be thought of as being incorporated into I_b, whereas the time course of I_{Ca} in our model very closely resembles the action potential clamp record (i.e., sum of I_{Ca} and I_{NaCa} and any Ca^{2+}-activated currents) obtained in the SA node when Ca^{2+} entry is blocked (120).

Other currents. Other currents, such as I_{st} [a sustained inward current, carried by Na^+, insensitive to TTX, and sensitive to Ca^{2+} channel blockers (71, but see Ref. 107)] and $I_{K(Ca)}$ [a Ca^{2+}-activated K^+ current, for which evidence is found only in the perforated-patch configuration (120)], exist in the SA node. Because there are no reports of these currents in ventricular cells, we do not include them in our model.

RESULTS

Spontaneous Activity

Action potentials recorded from 17 small clusters clearly show considerable cluster-to-cluster variability (Fig. 5) (17). Figure 6*A* shows a recording of V obtained from one small

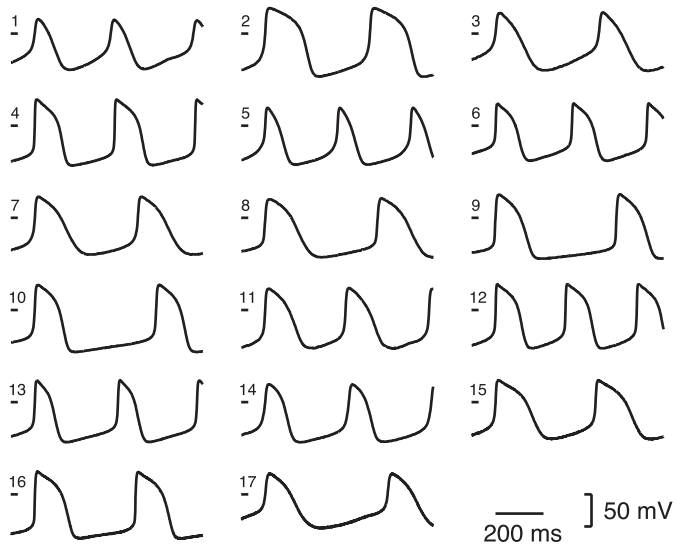

Fig. 5. Transmembrane potential recorded during spontaneous activity from *clusters 1–17*. Tic marks indicate 0 mV.

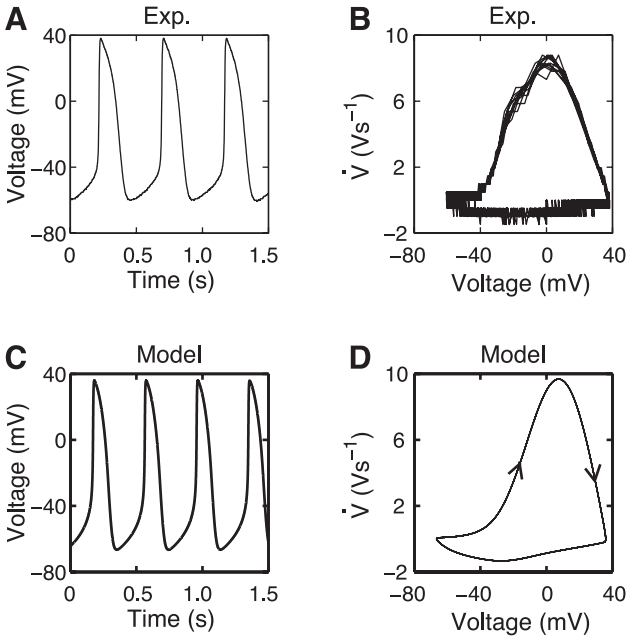

Fig. 6. *A*: transmembrane potential (V) recorded during spontaneous activity from 1 cell in a cluster (*cluster 7* in Fig. 5). *B*: phase-plane trajectory of 8 cycles in the cluster [dV/dt or maximum rate of rise of upstroke ($\dot{V}$) vs. V]. *C*: V during spontaneous activity in the model. *D*: phase-plane trajectory in the model (dV/dt or $\dot{V}$ vs. V). Initial conditions (see APPENDIX) closely approximate a point on the limit cycle corresponding to spontaneous activity. In *C* and *D*, a transient of 2 s was removed.

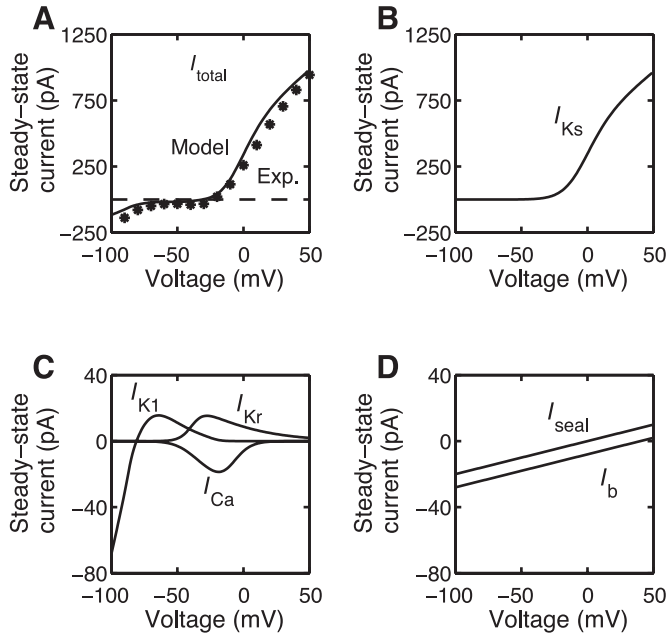

Fig. 7. Steady-state current-voltage (I-V) curves. *A*: steady-state I-V relation of total current (I_{total}) in experiments (Exp, ∗; $n = 5$) and model (curve). *B–D*: I-V curves of individual currents in the model. I_{scal}, seal-leak current; I_b, background current.

cluster (*cluster 7* in Fig. 5), whereas Fig. 6*B* shows the phase-plane trajectory, in which the rate of change of V ($\dot{V}$) is plotted vs. V. For this cluster, the mean values of the parameters, averaged over 100 cycles of activity, were as follows: IBI = 458 ms, MDP = −57 mV, APA = 89 mV, $\dot{V}_{max}$ = 7.5 V/s, DDR = 85 mV/s, APD_{50} = 124 ms, and APD_{100} = 224 ms. The action potential parameters (means ± SD) of the 17 clusters are given in Table 1. Because of beat-to-beat variability, the action potential parameters for each cluster were averaged over ~100 beats before the population average was taken. Figure 6, *C* and *D*, gives the voltage-time series and the phase-plane trajectory for the ionic model, and Table 1 gives the action potential parameters in the model, which are quite close to the mean experimental values.

Steady-State I-V Relations

The curve in Fig. 7*A* gives the steady-state I-V relation for the total current in the model. This curve corresponds closely to the mean I-V data points obtained from five 7-day ventricular clusters in our laboratory (Fig. 7*A*, symbols); see also Ref. 4. The steady-state I-V relations of the individual currents in the model are shown in Fig. 7, *B–D*.

Currents Underlying the Action Potential

We previously mentioned that the spontaneous activity in the model (Fig. 6, *C* and *D*) has action potential parameters that compare well with the mean experimental values (Table 1). Figure 8 shows V during approximately one cycle of spontaneous activity in the ionic model (*A*) and the various currents (*B–D*) and the various activation and inactivation variables (*E* and *F*). The upstroke phase is clearly generated by I_{Ca} (Fig. 8*C*), which rapidly activates (*d* in Fig. 8*E*, see also Fig. 1*B*). During the first third of the action potential, the slow activation of I_{Ks} (*n* in Fig. 8*F*, see Fig. 2*B*) contributes increasingly to repolarization (Fig. 8*C*); I_{Kr} is small (Fig. 8*C*), despite rapid activation (*s* in Fig. 8*F*, see Fig. 3*B*) because of its strong inward rectification (*z* in Fig. 8*F*, see Fig. 3*C*); there is also a smaller contribution from I_{seal}, which is outward but becomes less outward with time (Fig. 8*D*); I_b is inward and gradually becomes more inward with time (Fig. 8*D*); I_{K1} plays no role here (Fig. 8*D*) because of its strong inward rectification (K1 in Fig. 8*E*, see Fig. 7*C*). There is also a secondary increase of I_{Ca} (Fig. 8*C*), which serves to maintain the plateau phase of the action potential, despite decreased activation and increased inactivation of I_{Ca} (*d* and *f* in Fig. 8*E*); this is due to an increase in driving force. The overall shape of the waveform of I_{Ca} during the action potential resembles that seen in action po-

Table 1. *Action potential parameters: experiment vs. model*

	IBI, ms	$\dot{V}_{max}$,V/s	MDP, mV	APA, mV	DDR, mV/s	APD_{50}, ms	APD_{100}, ms
Experiment	389 ± 78	8.5 ± 4.6	−60 ± 4	93 ± 7	110 ± 30	108 ± 24	176 ± 39
Model	392	9.5	−67	102	90	108	181

IBI, interbeat interval; $\dot{V}_{max}$, maximum rate of rise of upstroke; MDP, maximum diastolic potential; APA, action potential amplitude; DDR, diastolic depolarization rate; APD_{50} and APD_{100}, action potential duration at 50 and 100% repolarization. For each cluster, mean values of action potential parameters were computed for a train of ~100 action potentials. Experimental values are means ± SD of these mean values for 17 clusters.

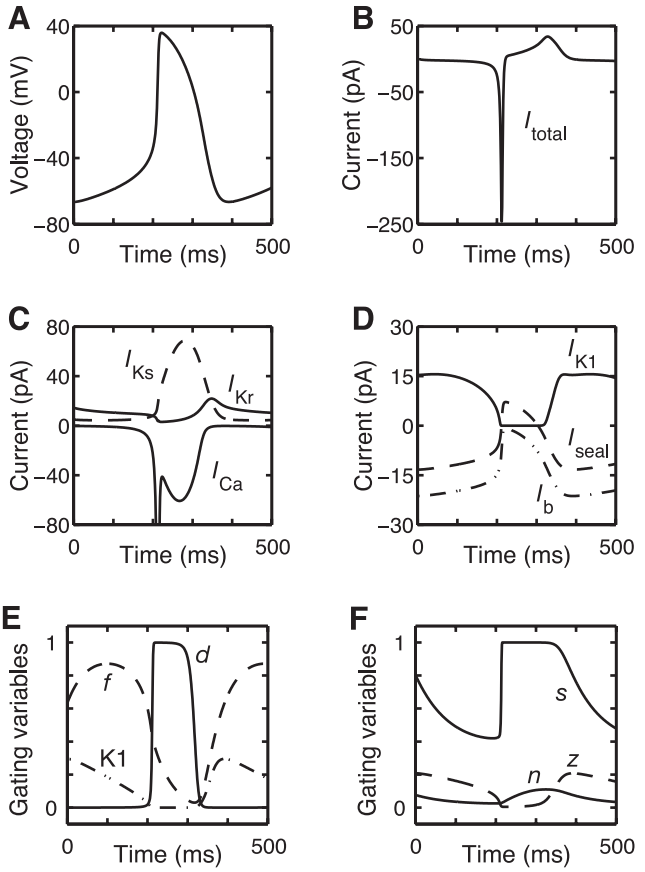

Fig. 8. Spontaneous activity in the model. *A*: transmembrane potential. *B*: total current. *C* and *D*: individual currents. Peak value of I_{Ca} is −262 pA (off-scale deflection in *C*). *E* and *F*: activation and inactivation variables in the model. Also shown is the function $z(V)$, describing rectification of I_{Kr}.

tential-clamp studies on SA node cells (120) and in some models of such cells (see Fig. 6 of Ref. 54). During the middle part of repolarization, I_{Ca}, after its secondary peak (Fig. 8*C*), falls as a result of inactivation and deactivation (*f* and *d* in Fig. 8*E*), which would per se promote repolarization. Because of a decrease in driving force, I_{Ks} decreases (Fig. 8*C*) and later starts to deactivate (*n* in Fig. 8*F*). There is also a fall in the outward I_{seal}, which eventually becomes an inward current (Fig. 8*D*). During the final stage of repolarization, there are contributions from I_{Kr} (Fig. 8*C*) and I_{K1} (Fig. 8*D*), which are no longer completely rectified (K1 and *z* in Fig. 8, *E* and *F*).

Currents Underlying the Pacemaker Potential

Because DDR in a three-cell cluster is ~100 mV/s (Table 1), the net current during diastolic depolarization is tiny (~2.6 pA); it is not even appreciable on the scale of Fig. 8*B*. I_{Ca} is inward and gradually becomes more inward throughout phase 4 depolarization (Fig. 8*C*), which agrees with the results from ruptured-patch action potential clamp studies on single SA node cells (120). I_b and I_{seal} are also inward throughout phase 4 depolarization but gradually become less inward (Fig. 8*D*). Although I_{Ks}, I_{Kr}, and I_{K1} are outward during phase 4 depolarization, I_{K1} becomes much less outward (Fig. 8*D*), I_{Ks} gradually becomes slightly less outward (not visible on the scale of Fig. 8*C*) but does not contribute much current, and I_{Kr} contributes increasingly less outward current as a result of slow deactivation (Fig. 8, *C* and *F*).

I_{Kr} deactivates slowly during diastolic depolarization (Fig. 8, *C* and *F*), because the time constant for activation (τ_s) is several hundred milliseconds over the pacemaker range of potentials (Fig. 3*B*). Hence, I_{Kr} is not fully deactivated by the beginning of the upstroke of the action potential. However, the increase in voltage during the upstroke rapidly abolishes I_{Kr} (Fig. 8*C*) because of its profound inward rectification (Figs. 3*C* and 8*F*). As the membrane then repolarizes, fast recovery from the inactivation of I_{Kr} is responsible for its rectification (Fig. 8*F*). The time course of I_{Kr} during spontaneous activity is very different from that seen in an atrial reaggregate model (see Fig. 15 of Ref. 89), where I_{Kr} deactivates much more rapidly because of its shorter time constant at the more hyperpolarized MDP of the reaggregate model: about −90 mV (89) vs. −67 mV (present study). However, action potential clamp studies of rabbit SA cells, which are more depolarized than the chick atrial reaggregate, show a time course of I_{Kr} very similar to that in our model (see Fig. 1*C* of Ref. 76), as do SA node models that incorporate a sharply rectifying I_{Kr} component (see Fig. 6, *D* and *E*, of Ref. 54).

Effect of Ca^{2+} Channel Blockers on Spontaneous Activity

Application of D-600, a Ca^{2+} channel blocker, on 7- to 10-day cells and small clusters in our laboratory results in the abolition of spontaneous activity (Fig. 9*A*), with mean resting potential of −36.2 mV (n = 14) (49). We observed similar results with another Ca^{2+} channel blocker, diltiazem (51). In Fig. 9*A*, a sharp microelectrode is used so that the cessation of spontaneous activity is not due to dialysis of the pipette contents against the intracellular medium, leading to effects such as current rundown.

Gradually increasing block of I_{Ca} in the model, starting at 45 s in Fig. 9*C*, gives a time course of the voltage that is similar to the experimentally observed effect of D-600, with the membrane eventually coming to rest at −37 mV at ~120 s when ~90% of I_{Ca} is blocked. Because D-600 blocks $I_{Ca,L}$ and because our nonseparable I_{Ca} is close to $I_{Ca,L}$, the modeling intervention is similar to the experimental intervention of applying an $I_{Ca,L}$ blocker. In the experiment and the model, loss of OS initially proceeds at a slow rate (from just after *arrow 1* to just after *arrow 3* in Fig. 9*C*); then the rate of loss accelerates just before spontaneous activity is extinguished (i.e., just after *arrow 3* in Fig. 9*C*). The MDP initially drifts slowly positive and then suddenly depolarizes much more quickly (starting at *arrow 2* in Fig. 9*C*) before spontaneous activity ceases. In the experiment and the model, the phase of more rapid loss of MDP precedes the phase of more rapid loss of OS. The upstroke velocity gradually decreases throughout the course of the block, and APD_{100} increases (Fig. 9, *B* and *D*). Effects in many ways opposite to those described above are seen in our laboratory with administration of a Ca^{2+} channel agonist (BAY K 8644): there are increases in $\dot{V}_{max}$, OS, DDR, and APD, as well as a hyperpolarization of MDP and the threshold or take-off potential, and a fall in IBI (28); these changes are also seen in the model.

Figure 9*E* gives the bifurcation diagram for I_{Ca} block, computed using XPPAUT (25). The bifurcation parameter is g_{Ca}, and the bifurcation variable is V. The periodic activity of

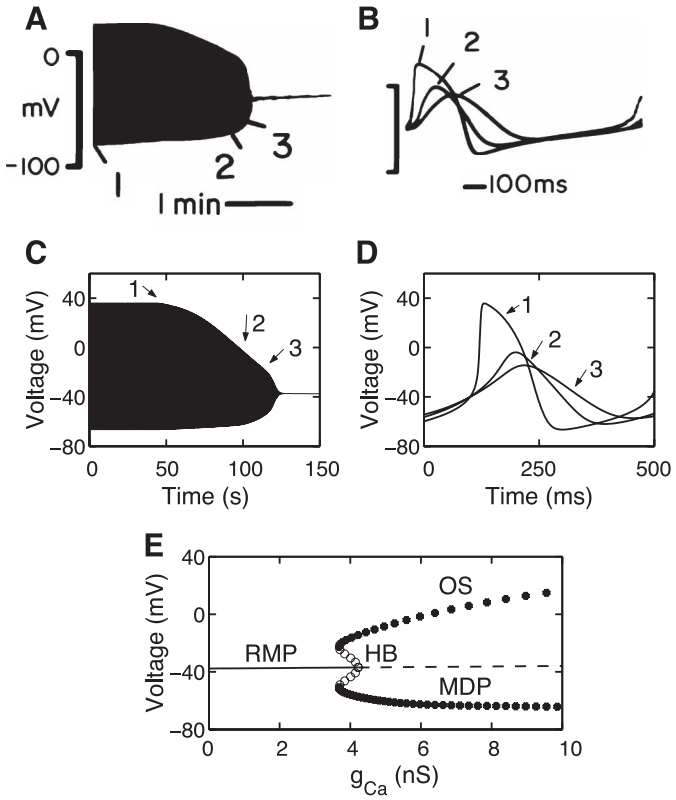

Fig. 9. Block of I_{Ca} (experiment and model). *A* and *B*: block of I_{Ca} with D-600 in experiments [adapted from Koidl and Tritthart (49)]. This preparation is thus not one of the 17 shown in Fig. 5; a sharp microelectrode was used. *C* and *D*: block of I_{Ca} in the model. Maximal conductance of I_{Ca} (g_{Ca}) was decreased linearly starting at 45 s at a rate of 0.36 nS/s. At ~120 s, when spontaneous activity stops, ~90% of g_{Ca} is blocked. *E*: bifurcation diagram with g_{Ca} as bifurcation parameter. For a steady state, the bifurcation variable is the voltage coordinate (V) of that point: solid line, stable [resting membrane potential (RMP)]; dashed line, unstable. For a limit cycle, maximum [i.e., overshoot potential (OS)] and minimum [i.e., maximal diastolic potential (MDP)] values of V are plotted: ●, stable; ○, unstable; HB, Hopf bifurcation.

the model corresponds to the existence of a stable limit cycle in the six-dimensional phase space of the system. As g_{Ca} is reduced from its nominal value of 30 nS, the limit cycle decreases in size, so that the APA falls: the maximum value of the V coordinate of the limit cycle (i.e., the OS) and its minimum value (i.e., the MDP) are shown in Fig. 9*E*. The locus of the V coordinate of the unstable steady state, which is also present in the phase space of the system and corresponds to the zero-current crossing of the total-current *I-V* curve in Fig. 7*A*, is also shown in Fig. 9*E* (dashed line). At $g_{Ca} = 4.2$ nS, a subcritical Hopf bifurcation (Fig. 9*E*) produces an unstable limit cycle oscillation, which grows in amplitude as g_{Ca} is reduced further, until the stable and unstable limit cycles collide at $g_{Ca} = 3.7$ nS in a reverse saddle-node bifurcation of limit cycles (31).

Relatively slow ("quasi-static") reduction in g_{Ca} from its control value of 30 nS (Fig. 9*C*) corresponds to moving from right to left along the stable limit-cycle branch of the bifurcation diagram in Fig. 9*E*. Eventually, at $g_{Ca} \approx 3.7$ nS, the state point will leave the stable periodic branch and move toward the stable steady state produced in the subcritical Hopf bifurcation. (The resting membrane potential corresponding to this stable steady state is shown in Fig. 9*E*.) This agrees with the simulation of Fig. 9*C*, where spontaneous activity is abolished with ~90% block of I_{Ca}. This "falling off" is responsible for the rapid phase of decline in the OS after *arrow 3* just before spontaneous activity is abolished in Fig. 9*C*. [This is also seen in the experiment (Fig. 9*A*).] In the model (Fig. 9*C*), the more rapid phase of decline of MDP starts earlier, before the falling off (just after *arrow 2*), at $g_{Ca} \approx 6$ nS, which agrees with the change in the slope of MDP in the bifurcation diagram (Fig. 9*E*). [This pattern is also seen in the experiment (Fig. 9*A*).] When a trace such as that shown in Fig. 9*C*, with distinct phases of change of MDP and OS, is seen experimentally, one should begin to think that abolition of spontaneous activity might involve a subcritical, rather than a supercritical, Hopf bifurcation.

The coexistence of a stable limit cycle and a stable steady state for 3.7 nS $< g_{Ca} <$ 4.2 nS in Fig. 9*E* implies that, over this range, one should be able to trigger activity from the resting state by injecting a stimulus and that this activity should be annihilated by injection of a single well-timed stimulus (31). We have indeed observed single-pulse triggering and annihilation in the model at $g_{Ca} = 3.9$ nS. Annihilation has been seen in isolated ventricular cells (94) and in reaggregates of atrial cells exposed to TTX (90). We do not know whether the bistable range in Fig. 9*E* would be wide enough in the experiment to allow observation of single-pulse triggering and annihilation in these clusters, because this would necessitate adjustment of the D-600 concentration to a value within a rather narrow range, which will be different from cluster to cluster and will be unknown a priori. However, other experimental evidence supports the scenario of Fig. 9*E*.

The existence of a saddle-node bifurcation in Fig. 9*E* is consistent with three prior observations from our laboratory: *1*) During washout of D-600, transient flurries of action potentials occur spontaneously before spontaneous activity is permanently reestablished. The amplitude of the first action potential in each flurry is relatively large, with the amplitude of the following action potentials gradually declining during the course of each episode of transient triggered activity (see Fig. 2*C* of Ref. 49). *2*) Once beating has stopped under the influence of diltiazem, injection of a hyperpolarizing bias current can provoke an episode of transient triggered activity, with the first action potential being an anodal-break response (see Fig. 2 of Ref. 51). As time proceeds and the degree of block continues to increase during quiescence, the number of action potentials in an episode decreases. This "critical slowing-down" behavior is consistent with the existence of a saddle-node bifurcation of limit cycles and can be seen in simulations with the model. *3*) In some cells that are initially found to be not spontaneously active, injection of a single hyperpolarizing current pulse again elicits a flurry of triggered action potentials, with the action potential amplitude gradually decreasing during each flurry (see Figs. 4 and 6 of Ref. 49). During ongoing superfusion of these cells with D-600, the number of nondriven action potentials in any one trial gradually decreases from tens of action potentials, then the membrane does not produce triggered action potentials, and finally the membrane becomes inexcitable (see Fig. 4 of Ref. 49).

A response similar to that shown in Fig. 9, *A–D*, is seen with $I_{Ca,L}$ block in the SA node in experiments (see references in Ref. 31) and in several ionic models (31, 54, 55). However, in some of these SA node models, a supercritical Hopf bifurcation

occurs, so that annihilation and single-pulse triggering cannot occur.

Effect of Almokalant on Spontaneous Activity

Addition of 1 or 2 mM almokalant, a specific blocker of I_{Kr} (113), to the bath results in a slowing of the terminal rate of repolarization, a small depolarization of the MDP, and a slight loss of OS (Fig. 10*A*).

In the model, 100% block of I_{Kr} (Fig. 10*B* shows 50%, as well as 100%, block of I_{Kr}) results in a marked depolarization of MDP, a slight slowing of the terminal rate of repolarization, a small increase in APD_{100}, a decrease in APD_{50}, a decrease in IBI, a fall in $\dot{V}_{max}$, and a decrease in OS. The slowing of the terminal rate of repolarization and the depolarization of the MDP are due to the absence of the I_{Kr} contribution normally present (see I_{Kr} trace in Fig. 8*C* during control activity). The resultant relative depolarization then causes I_{Ks} to remain considerably more outward during the entire pacemaker potential and even during the early part of the action potential (Fig. 10*C* shows I_{Ks} time course during 100% I_{Kr} block), which is the major cause of the decrease in APD_{50} in Fig. 10*B*. This secondary increase in I_{Ks} also accounts for the relatively small effect of the loss of I_{Kr} on the rate of terminal repolarization in Fig. 10*B*. In cells that do not have I_{Ks}, this indirect effect of I_{Kr} block on I_{Ks} would not occur, and one would expect a prolongation of APD, as observed in SA node cells in which I_{Ks} was not found (106). [In later studies, however, I_{Ks} was clearly found in SA node cells (59, 110).] The fall in $\dot{V}_{max}$ and OS is due to a decrease in I_{Ca}, with a fall in peak value from 263 to 207 pA during 100% I_{Kr} block as a result of greater inactivation of I_{Ca} during diastolic depolarization. Similarly, in experiments on the SA node, effects on action potential parameters due to selective block of I_{Kr} with the compound E-4031 have been found to be due to "a combination of direct and indirect effects on various ionic currents" (106).

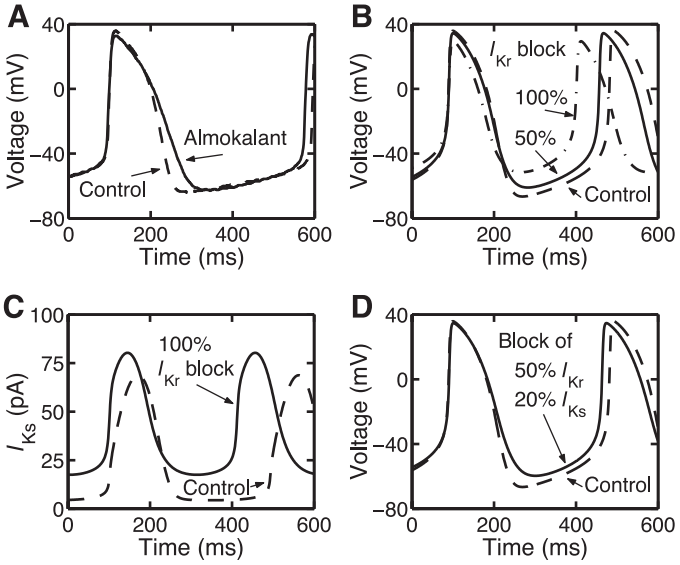

Fig. 10. Effect of almokalant (experiment and model). *A*: effect of almokalant on *cluster 9* in Fig. 5 (solid line) vs. control (dashed line). *B*: effect of block of 50% (solid line) and 100% (dashed-dotted line) of I_{Kr} in the model. *C*: I_{Ks} during 100% block of I_{Kr} in the model (solid line). *D*: effect of 50% block of I_{Kr} and 20% block of I_{Ks} in the model (solid line; latter to simulate rundown).

The shortening of APD_{50} in the model with I_{Kr} block (Fig. 10*B*) does not occur in the experiment (Fig. 10*A*). One reason that might account for this discrepancy is the rundown of I_{Ks} that occurs during the 10-min period between rupture of the patch (to enter whole cell recording mode) and initiation of the recording of the effect of almokalant (79). Figure 10*D* shows the combined effect in the model of 50% block of I_{Kr} (to simulate almokalant) and 20% block of I_{Ks} [to simulate the degree of rundown seen experimentally (79)]: APD_{50} is no longer decreased.

To avoid the above-mentioned artifact due to dialysis of cytoplasm against the pipette contents and rundown of currents, we also used visual monitoring of mechanical beating to assess the effect of almokalant. Although three clusters stopped beating on exposure to almokalant (and the effect was reversible on washout of almokalant from the bath), another four clusters did not stop beating: IBI was increased in three of four clusters, and there was no change in the remaining cluster. In response to 0.1 μM E-4031, another specific I_{Kr} blocker, half of the single SA node cells stopped beating in one study (106), whereas none stopped in another study (76). When the concentration was raised to 1.0 μM, at which there are still negligible effects on other currents, all cells ceased spontaneous activity in both studies. A similar response was found in small balls of tissue isolated from the SA node: with 1.0 μM E-4031, activity was abolished in all balls; with 0.1 μM E-4031, activity was sometimes extinguished in balls from the central area, but not in those from more peripheral areas (46). The fact that 0.1 μM E-4031 abolishes spontaneous activity in smaller, but not in larger, single SA node cells agrees with this observation (59), provided that small cells do indeed stem from the central area of the node and larger cells stem from the periphery.

Complete block of I_{Kr} does not abolish spontaneous activity in the model (Fig. 10*B*). In contrast, cessation of spontaneous activity does occur with complete I_{Kr} block in some SA node models, sometimes via a supercritical Hopf bifurcation, sometimes via what is probably a subcritical Hopf bifurcation, and sometimes through an intermediary phase of "irregular dynamics" (see Fig. 13 of Ref. 54).

Effect of Ba^{2+} on Spontaneous Activity

In 7-day ventricular cells, a low concentration of Ba^{2+} (0.2 mM) blocks I_{K1} without greatly affecting I_{Ks} and I_{Kr} (8). Figure 11*A* shows the effect of 0.1 mM Ba^{2+} in an experiment, and Fig. 11*B* shows the effect of blocking I_{K1} completely in the model. In the experiment and the model, there is a depolarization of MDP, a decrease in $\dot{V}_{max}$, a loss of OS, and a decrease in IBI. With the average drift of action potential parameters in control recordings after 10 min (the time after which the effects due to Ba^{2+} were measured) taken into account, MDP depolarizes by 5%, $\dot{V}_{max}$ decreases by 13%, APA decreases by 7%, and IBI decreases by 9% ($n = 4$) (79), whereas in the model, MDP depolarizes by 15%, $\dot{V}_{max}$ decreases by 28%, APA decreases by 13%, and IBI decreases by 11%. However, the increases in APD and DDR in the experiments (12% increase in APD_{50} and 28% increase in APD_{90}) are not replicated in the model. Because we have observed neither an increase in the peak I_{Ca} nor slowed inactivation kinetics of I_{Ca} with elevated Ba^{2+} (79), we attribute the increase in APD in the experiments

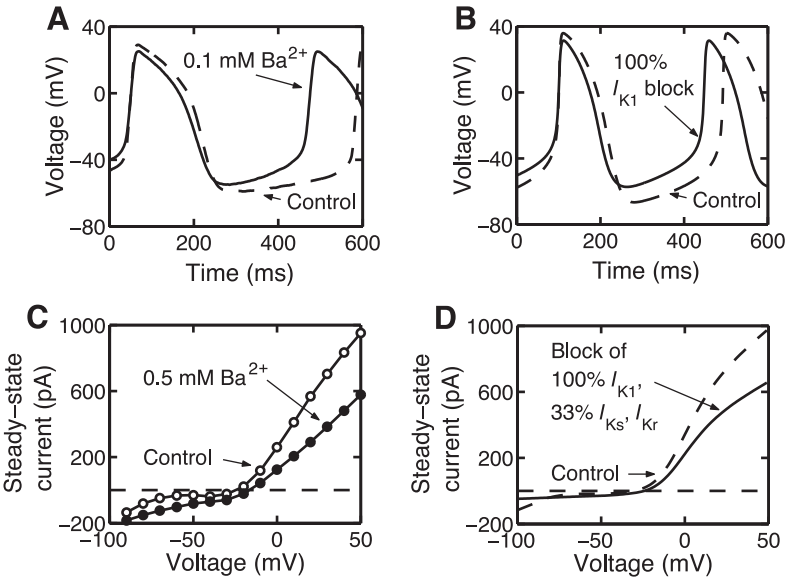

Fig. 11. Effect of Ba^{2+} (experiment and model). *A*: effect of 0.1 mM Ba^{2+} on spontaneous activity in a cluster (solid line) vs. control (dashed line). Cluster is not among those (*clusters 1–17*) in Fig. 5. *B*: effect of 100% I_{K1} block (solid line) vs. control (dashed line) in the model. *C*: steady-state *I-V* curve with 0.5 mM Ba^{2+} (●) and in control (○). Values are means of 9 clusters, none of which are shown in Fig. 5. *D*: steady-state *I-V* curve with 100% block of I_{K1} and 33% block of I_{Ks} and I_{Kr} (solid line) vs. control *I-V* (dashed line) in the model.

at least partially to rundown of I_{Ks}, as we observed with almokalant (see *Effect of Almokalant on Spontaneous Activity*).

Increasing Ba^{2+} to 0.5–1.0 mM results in partial block of I_{Ks} (8, 79) and I_{Kr} (79), in addition to complete block of I_{K1}. Figure 11*C* shows the mean effect ($n = 9$) on the steady-state *I-V* relation when 0.5 mM Ba^{2+} is applied to small clusters. Figure 11*D* shows the effect on the steady-state *I-V* relation in the model of 100% block of I_{K1}, 33% block of I_{Ks}, and 33% block of I_{Kr}. (The degree of block of I_{Ks} and I_{Kr} in the model was chosen to make the blocked current comparable with the combined effects of rundown and Ba^{2+} in Fig. 11*C*). The steady-state *I-V* curve is no longer N-shaped. The effect on spontaneous activity in the experiment and the model is a more marked change from control in the action potential parameters than at the lower Ba^{2+} concentration (Fig. 11, *A* and *B*). Specifically, in the experiment, again with the average drift over a period of 10 min in action potential parameters in control recordings taken into account, the MDP depolarizes by 11%, $\dot{V}_{max}$ decreases by 49%, APA decreases by 15%, and IBI decreases by 34% ($n = 8$) (79), whereas in the model, MDP depolarizes by 27%, $\dot{V}_{max}$ decreases by 39%, APA decreases by 23%, and IBI decreases by 20%.

At an even higher concentration (1 mM), Ba^{2+} abolishes spontaneous activity in the clusters, with the membrane coming to rest at about −35 mV (79). The effect is reversible, in that spontaneous activity resumes with washout of Ba^{2+}. Depolarization of MDP and cessation of spontaneous activity have previously been described in 6- to 7-day ventricular cells exposed to 5–10 mM Ba^{2+} (96). Cessation of spontaneous activity is also seen in the model if, in addition to complete block of I_{K1}, I_{Ks} and I_{Kr} are blocked by 68%, with the membrane coming to rest at −17 mV. In this case, the activity is abolished through a supercritical Hopf bifurcation. This modeling result agrees with there being only one distinct phase of change of MDP and OS in the experiment (79), in contrast to the result of I_{Ca} block (Fig. 9). Blocking the other background current in the model (I_b) results in the cessation of spontaneous activity via an infinite-period bifurcation.

Effect of I_{seal} on Spontaneous Activity

It is possible that I_{seal} is essential for the generation of spontaneous activity in our model. However, when I_{seal} is removed, spontaneous beating continues in the model, although at a considerably increased IBI of 535 ms and a more hyperpolarized MDP of −72 mV (Fig. 12). This result agrees with the fact that we record from clusters that are seen to be beating before they are subjected to patching; i.e., the depolarizing I_{seal} does not induce spontaneous beating in our clusters. However, patching onto a single cell can change the IBI or even abolish preexisting spontaneous activity (112). Indeed, if our model (with the nominal seal-leak resistance of 5 GΩ) is reformulated for a single cell (i.e., capacitance = 8.5 pF), the MDP depolarizes to −51 mV and the IBI decreases to 293 ms; with a seal-leak resistance of 3 GΩ, spontaneous activity is abolished in the single-cell model.

We have used a nominal seal-leak resistance of 5 GΩ in our model (20). This is a worst-case scenario, because 5 GΩ is toward the lower end of the range of values reported in experimental work on chick cells (42, 63, 79). When the seal-leak resistance in the model is increased to 20 GΩ, which is toward the higher end of that used in our laboratory (79), IBI increases from 392 to 475 ms. Thus differences in seal-leak resistance might account for part of the prepara-

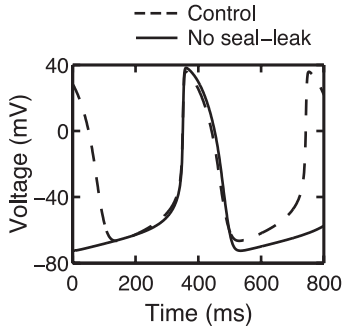

Fig. 12. Effect of removal of I_{seal} in the model.

tion-to-preparation differences in IBI and DDR seen experimentally (Fig. 5).

DISCUSSION

Spontaneous Activity in Isolated Chick Ventricular Cells

Electrical recordings of spontaneous activity in single embryonic chick ventricular cells, in small clusters of such cells, and in sparse monolayers have been made using conventional sharp microelectrodes (17, 26, 48, 49, 51, 78, 95) or patch pipettes in the whole cell recording mode (64, 67, 112). Among these studies, those that use 7-day ventricular cells at an external $[K^+]$ of 2.7–5.4 mM generally report that the cells have an MDP between −60 and −70 mV and a slow upstroke velocity of ~10 V/s. One systematic study, which used sharp microelectrodes, reported MDP of −68.4 ± 1.0 mV and OS of 22 ± 0.9 mV ($n = 30$) at an external $[K^+]$ of 4.2 mM (17). Our findings in small clusters (Table 1) are in agreement with the findings of these previous studies.

How does the electrical activity of small clusters compare with that of the in situ ventricular muscle? The APA and APD of our small clusters (and in the other reports on single cells, small clusters, and sparse monolayers mentioned above) are quite similar to those of in situ ventricular muscle (98, 101, 118). In contrast, in situ ventricular muscle, with one exception (97), has not been reported to show spontaneous phase 4 depolarization (61, 101, 118) and has a much larger $\dot{V}_{max}$: 70–94 V/s at 5–7 days (19, 98, 118) vs. 8.5 V/s (present study). The absence of diastolic depolarization in the in situ 7-day chick ventricle could be due to overdrive suppression, because, in the only report in which pacemaker potentials were seen in intact 7-day ventricles, such potentials were seen in only 20–40% of intact ventricles but in 100% of cut 7-day ventricular fragments (97). Alternatively, the dissociation procedure or the time spent in culture (104) could change the electrophysiological properties of cultured cells. Adding the I_{Na} known to be present in the small clusters to the model (see METHODS) and increasing I_{K1} to the point where spontaneous activity stops with a resting membrane potential of −73 mV give a $\dot{V}_{max}$ of an induced action potential of 54 V/s, suggesting that the low value of $\dot{V}_{max}$ in the clusters is indeed due to virtually complete inactivation of I_{Na}.

The action potential parameters of 7-day embryonic chick ventricular cells are very close to those of isolated SA node cells (compare data in Table 1 with data from the many experimental studies summarized in Table 1 of Ref. 54). This is not too surprising, given that a similar mix of currents seems to be present in the central part of the SA node and in our cells. For example, in the smallest SA node cells (presumably from the central part of the node), which have a capacitance about the same as one of our three-cell clusters (i.e., ~20 pF), currents such as $I_{Ca,L}$, I_{Kr}, and I_{Ks} and background currents are present, but other currents such as I_{Na}, I_f, and $I_{Ca,T}$ are absent or the membrane is too depolarized to allow activation (e.g., I_f) or to allow removal of inactivation (e.g., I_{Na}) (36). Indeed, a minimal SA node model with only I_{Ca}, I_K, and a background current produces very respectable-looking spontaneous activity (33).

Currents Underlying Diastolic Depolarization in the Model

A DDR of ~100 mV/s (Table 1) in a three-cell cluster with a capacitance of 25.5 pF requires that the net current flowing during spontaneous diastolic depolarization be 2.55 pA. In our model, this net current is obtained from the algebraic sum of several much larger inward and outward currents (Fig. 8). In models of SA node cells, these individual currents contribute to various extents to produce this tiny net current (see Fig. 4 of Ref. 115 and Figs. 6 and 7 of Ref. 54). At present, we have no way of knowing exactly which currents are flowing and in what amounts during diastolic depolarization in a given cell; to make matters worse, this mix of currents almost certainly changes from cell to cell, especially in cells from structures as inhomogeneous as the SA node (47).

The current for which we have the least direct experimental evidence in our model is I_b (14). We have added this current to the model, because we know that an inward background current is needed to generate a steady-state *I-V* curve that agrees with the experiment (Fig. 7*A*) and to allow the membrane to come to rest at about −40 mV when I_{Ca} is blocked (Fig. 9). Background currents have also been described in SA node cells (34, 106). One or more inward background currents are incorporated into all models of atrial (9, 52, 88–90) and ventricular (11, 88) reaggregates, as well as into all models of SA node cells (see Fig. 4 of Ref. 115 and Fig. 7 of Ref. 54). As in many of the above-mentioned models, the inward background current is necessary for spontaneous activity in our model, in that deletion of the inward background current results in the cessation of spontaneous activity.

Very early during development (3 days), the steady-state inactivation curve of I_{Na} is shifted in the depolarizing direction (82); simulations suggest that the window component of I_{Na} might then contribute to diastolic depolarization (83). I_{st} has been reported during diastolic depolarization in spontaneously active single SA node cells (71, but see Ref. 107); intriguingly, I_{st} is not present in quiescent SA node cells (71). We know of no reports of I_{st} in embryonic chick cells.

I_{seal} injected through the gigaohm seal-leak resistance is a source of artifact in our experimental recordings. This is true even if the perforated-patch, rather than the ruptured-patch, technique were to be used. In contrast to the case in relatively large adult mammalian ventricular cells with input resistances on the order of tens of megohms, I_{seal} has significant effects when smaller cells (e.g., SA node cells and embryonic cells) with membrane resistances on the order of 1 GΩ at −70 mV [as do our clusters; see also Ref. 29] are studied (20). It is thus conceivable that I_{seal} is causing depolarization to the point that I_{Na} and $I_{Ca,T}$, although present, become inactivated and I_f becomes deactivated. However, in our model, subtraction of I_{seal} hyperpolarizes the MDP by only 6 mV (resp. 2 mV) while increasing the IBI from 392 to 535 ms (resp. 472 ms) when the seal-leak resistance is 5 GΩ (resp. 20 GΩ). This extra hyperpolarization is not sufficient to activate significant amounts of I_{Na}, because when I_{Na} is added to the model (see METHODS), removal of the 5-GΩ seal-leak resistance results in a decrease in IBI from 392 to 533 ms and an increase in $\dot{V}_{max}$ from 10.2 to 10.9 V/s. Similarly, when I_f is added to

the model (see METHODS), the extra hyperpolarization does not activate I_f significantly: in this case, removal of I_{seal} increases the IBI from 390 to 520 ms.

Spontaneous Activity: Cell-to-Cell Variability and Activity-Dependent Conductances

There is considerable variability in electrical parameters from cluster to cluster (Fig. 5). The extent to which this is a result of true inhomogeneity within the cellular population [e.g., the regional heterogeneities in the early embryonic chick heart (1, 101) and the apex-to-base and endocardial-to-epicardial ventricular gradients known to be present in adult muscle (77)] is not clear. There is almost certainly an artifact stemming from differences in dissociation conditions from one culture to another (and even from cluster to cluster within the same culture). I_{seal} is also different from cluster to cluster. Population inhomogeneity exists in ventricular cells isolated from the adult rat heart (77) and the adult guinea pig heart (119), as well as in cells isolated from the rabbit SA node (75). Although at first sight these cell-to-cell differences might appear to be so large as to be problematic for physiological function, experimental and modeling work indicates that cell-to-cell differences in APD would be largely smoothed out in situ by gap-junctional coupling (119); a similar conclusion holds for IBI (108).

The action potential parameters in the model are very close to the mean values obtained in the experiment (Table 1). However, because of the inhomogeneity of the cellular population, a particular action potential parameter in a given cluster can be quite different from that in the model. For example, in Fig. 5 the MDP in the model is more depolarized than in *cluster 16*, the IBI is much smaller than in *cluster 17*, and the APD is much shorter than in *cluster 2*. In each of these cases, the model could presumably be modified to replicate the electrical activity in the particular cluster by changing particular currents (e.g., increasing the conductance of one or more of the K^+ currents to produce a more hyperpolarized MDP or increasing the conductance of I_{Ca} to extend the APD). However, this is an exercise in "theorizing in a vacuum," given that one does not know (and cannot know, with the available technology) the exact parameters describing all the ionic currents in a given cell.

The wide variety of shapes of the action potentials seen in the experiment and the corresponding cell-to-cell variability in the individual currents must mean that the currents influencing APD and DDR (and, hence, IBI) are mixed to various extents in different clusters. Because ~40% of our clusters do not beat (50), it is perhaps not surprising that there is a great deal of cluster-to-cluster variability in IBI and in the waveform of the action potential. It has been suggested that activity-dependent conductances might provide a negative-feedback mechanism by which spontaneous activity can be regulated (for review see Ref. 80). It is quite conceivable that some such homeostatic process is occurring here, because, e.g., it is known that messenger RNA expression and protein level of one K^+ channel are decreased as a result of KCl-induced depolarization in pituitary cells (60). It is also possible that the individual currents, through their voltage dependence, negatively feed back on each other to regulate spontaneous activity (73).

Limitations of the Model

Our first-generation model contains no pumps or exchangers and has fixed ionic concentrations. It thus cannot be used to realistically model phenomena such as the rise in internal $[Na^+]$ seen when I_{NaK} is blocked or the change in internal $[Ca^{2+}]$ that occurs should IBI be changed. Because data are not available for all the currents in 7-day embryonic chick ventricular cells, there are uncertainties in some of the currents: I_{Kr} is taken from experiments on atrial reaggregates, and we use a nonseparable I_{Ca}. Although we have used the classic Hodgkin-Huxley description for the gating of all the currents in our model, there are channels that do not always behave in this way, e.g., the "bursting" mode of I_{Na}, which occasionally results in a longer-lasting current (40, 64). As in all work on ionic models of spontaneously active cells, I_b, which in our case is a composite current (including, e.g., I_{NaK}), is titrated to produce a reasonable IBI. There is evidence from recent work on the SA node that internal Ca^{2+} cycling contributes to generating spontaneous diastolic depolarization (56). Because there is no firm experimental evidence for this mechanism in embryonic chick ventricular cells, we do not entertain this possibility in our model.

The deterministic Hodgkin-Huxley-type model we present here shows no beat-to-beat fluctuation in action potential parameters. In contrast, all of our experimental recordings show considerable beat-to-beat fluctuations in the various action potential parameters (e.g., IBI). Previous modeling studies of rabbit SA node cells showed that the beat-to-beat fluctuations observed experimentally can be accounted for by the stochastic opening and closing of membrane channels (32, 114). Development of a stochastic single-channel version of the deterministic model we have described above allows investigation of this hypothesis (unpublished observations).

APPENDIX

Model Equations

Some model parameters (maximal conductances, reversal potentials, and capacitance) are given in Table 2.

Membrane Potential

$$dV/dt = -(I_{Ca} + I_{Ks} + I_{Kr} + I_{K1} + I_b + I_{seal})/C_m$$

Table 2. *Model parameters*

Parameter	Definition	Value
g_{Ca}	Maximal I_{Ca} conductance	30 nS
g_{Ks}	Maximal I_{Ks} conductance	7.8 nS
g_{Kr}	Maximal I_{Kr} conductance	6.0 nS
g_{K1}	Maximal I_{K1} conductance	3.6 nS
g_b	Maximal I_b conductance	0.2 nS
g_{seal}	Maximal I_{seal} conductance	0.2 nS
E_{Ca}	Reversal potential of I_{Ca}	40 mV
E_{Ks}	Reversal potential of I_{Ks}	−75 mV
E_{Kr}	Reversal potential of I_{Kr}	−81 mV
E_{K1}	Reversal potential of I_{K1}	−81 mV
E_b	Reversal potential of I_b	40 mV
E_{seal}	Reversal potential of I_{seal}	0 mV
C_m	Membrane capacitance	25.5 pF

I_{Ca}, Ca^{2+} current; I_{Ks}, slow delayed K^+ current; I_{Kr}, rapid delayed rectifier K^+ current; I_{K1}, inward rectifier K^+ current; I_b, background current; I_{seal}, seal-leak current.

Slow Inward Ca^{2+} Current

$$I_{Ca} = g_{Ca} d f (V - E_{Ca})$$

$$\frac{dd}{dt} = \frac{1}{\tau_d}(d_\infty - d)$$

$$\frac{df}{dt} = \frac{1}{\tau_f}(f_\infty - f)$$

$$f_\infty = 1/\{1 + \exp[(V + 42.8)/8.4]\}$$

$$d_\infty = 1/\{1 + \exp[-(V + 10.0)/6.2]\}$$

$$\tau_d = 0.001 \times \{1 - \exp[-(V + 10)/6.24]\}/(\{1 + \exp[-(V + 10)/6.24]\} \times [0.035(V + 10)])$$

$$\tau_f = 0.001/(0.0197\exp\{-[0.0337(V + 10)]^2\} + 0.02)$$

Slow Delayed K^+ Current

$$I_{Ks} = g_{Ks} n (V - E_{Ks})$$

$$\frac{dn}{dt} = \alpha_n(1 - n) - \beta_n n$$

$$\alpha_n = (2/3) \times 0.08(V - 15)/\{1 - \exp[-0.08(V - 15)]\}$$

$$\beta_n = (2/3) \times 0.156\exp[-0.055(V - 15)]$$

Rapid Delayed Rectifier K^+ Current

$$I_{Kr} = g_{Kr} s z(V)(V - E_{Kr})$$

$$z(V) = 1/\{1 + \exp[(V + 100)/25]\}$$

$$\frac{ds}{dt} = \alpha_s(1 - s) - \beta_s s$$

$$\alpha_s = 23.0\exp[0.13(V + 9.0)]$$

$$\beta_s = 0.036\exp[-0.09(V + 9.0)]$$

Inward Rectifier K^+ Current

$$I_{K1} = g_{K1} K1 (V - E_{K1})$$

$$\frac{dK1}{dt} = \alpha_{K1}(1 - K1) - \beta_{K1} K1$$

$$\alpha_{K1} = 1{,}000 \times 1.02/\{1 + \exp[0.2385(V - E_{K1} - 59.215)]\}$$

$$\beta_{K1} = 1{,}000 \times \{0.49124\exp[0.08032(V - E_{K1} + 5.476)] + \exp[0.06175(V - E_{K1} - 594.31)]\}/\{1 + \exp[-0.5143(V - E_{K1} + 4.753)]\}$$

Background Current

$$I_b = g_b(V - E_b)$$

Seal-Leak Current

$$I_{seal} = g_{seal}(V - E_{seal})$$

Voltages are in millivolts, currents in picoamperes, conductances in nanosiemens, capacitance in nanofarads, and time in seconds. The initial conditions are $V = -66.5526$ mV, $d = 1.0932 \times 10^{-4}$, $f = 0.6309$, $n = 0.0764$, $s = 0.8019$, and $K1 = 0.2953$.

ACKNOWLEDGMENTS

We thank Petra Lang for expert technical assistance and Prof. Erik Mosekilde (Technical University of Denmark), Prof. Michael Mackey (McGill University), and Prof. Helmut Tritthart (Medical University Graz) for facilitating our collaborative work.

GRANTS

This work was supported by Austrian Science Fund Operating Grant P 15403 (to B. Koidl) and Canadian Institutes for Health Research (CIHR) Operating Grant MOP-43846 (to M. R. Guevara). M. R. Guevara thanks the Medical Research Council of Canada for a Sabbatic Leave Research Grant (1992-93), and T. Krogh-Madsen thanks the CIHR, the Danish Research Agency, and Otto Mønsted's Foundation for predoctoral financial support.

REFERENCES

1. **Barry A.** The intrinsic pulsation rates of fragments of the embryonic chick heart. *J Exp Zool* 91: 119–130, 1942.
2. **Baruscotti M, DiFrancesco D, and Robinson RB.** Na^+ current contribution to the diastolic depolarization in newborn rabbit SA node cells. *Am J Physiol Heart Circ Physiol* 279: H2303–H2309, 2000.
3. **Bernus O, Wilders R, Zemlin CW, Verschelde H, and Panfilov AV.** A computationally efficient electrophysiological model of human ventricular cells. *Am J Physiol Heart Circ Physiol* 282: H2296–H2308, 2002.
4. **Brochu R.** *Pacemaking in Embryonic Chick Heart* (Master's dissertation). Montreal, PQ, Canada: McGill University, 1990.
5. **Brochu RM, Clay JR, and Shrier A.** Pacemaker current in single cells and in aggregates of cells dissociated from the embryonic chick heart. *J Physiol* 454: 503–515, 1992.
6. **Bub G, Glass L, Publicover NG, and Shrier A.** Bursting calcium rotors in cultured cardiac myocyte monolayers. *Proc Natl Acad Sci USA* 95: 10283–10287, 1998.
7. **Cavalié A, McDonald TF, Pelzer D, and Trautwein W.** Temperature-induced transitory and steady-state changes in the calcium current of guinea pig ventricular myocytes. *Pflügers Arch* 405: 294–296, 1985.
8. **Clapham DE and Logothetis DE.** Delayed rectifier K^+ current in embryonic chick heart ventricle. *Am J Physiol Heart Circ Physiol* 254: H192–H197, 1988.
9. **Clay JR, Brochu RM, and Shrier A.** Phase resetting of embryonic chick atrial heart cell aggregates. Experiment and theory. *Biophys J* 58: 609–621, 1990.
10. **Clay JR and DeHaan RL.** Fluctuations in interbeat interval in rhythmic heart-cell clusters. Role of membrane voltage noise. *Biophys J* 28: 377–389, 1979.
11. **Clay JR, Guevara MR, and Shrier A.** Phase resetting of the rhythmic activity of embryonic heart cell aggregates. Experiment and theory. *Biophys J* 45: 699–714, 1984.
12. **Clay JR, Hill CE, Roitman D, and Shrier A.** Repolarization current in embryonic chick atrial heart cells. *J Physiol* 403: 525–537, 1988.
13. **Clay JR, Kristof AS, Shenasa J, Brochu RM, and Shrier A.** A review of the effects of three cardioactive agents on the electrical activity from embryonic chick heart cell aggregates: TTX, ACh, and E-4031. *Prog Biophys Mol Biol* 62: 185–202, 1994.
14. **Clay JR and Shrier A.** Analysis of subthreshold pace-maker currents in chick embryonic heart cells. *J Physiol* 312: 471–490, 1981.
15. **Clay JR and Shrier A.** Developmental changes in subthreshold pace-maker currents in chick embryonic heart cells. *J Physiol* 312: 491–504, 1981.
16. **Colizza D, Guevara MR, and Shrier A.** A comparative study of collagenase- and trypsin-dissociated embryonic heart cells: reaggregation, electrophysiology, and pharmacology. *Can J Physiol Pharmacol* 61: 408–419, 1983.
17. **DeHaan RL and Gottlieb SH.** The electrical activity of embryonic chick heart cells isolated in tissue culture singly or in interconnected cell sheets. *J Gen Physiol* 52: 643–665, 1968.
18. **DeHaan RL and Hirakow R.** Synchronization of pulsation rates in isolated cardiac myocytes. *Exp Cell Res* 70: 214–220, 1972.
19. **DeHaan RL, McDonald TF, and Sachs HG.** Development of tetrodotoxin sensitivity of embryonic chick heart cells in vitro. In: *Developmental and Physiological Correlates of Cardiac Muscle*, edited by Lieberman M and Sano T. New York: Raven, 1975, p. 155–168.
20. **DiFrancesco D.** The contribution of the "pacemaker" current (i_f) to generation of spontaneous activity in rabbit sino-atrial node myocytes. *J Physiol* 434: 23–40, 1991.
21. **Dokos S, Celler BG, and Lovell NH.** Modification of DiFrancesco-Noble equations to simulate the effects of vagal stimulation on in vivo mammalian sinoatrial node electrical activity. *Ann Biomed Eng* 21: 321–335, 1993.
22. **Ebihara L and Johnson EA.** Fast sodium current in cardiac muscle. A quantitative description. *Biophys J* 32: 779–790, 1980.

23. **Endresen LP, Hall K, Hoye JS, and Myrheim J.** A theory for the membrane potential of living cells. *Eur Biophys J* 29: 90–103, 2000.
24. **Endresen LP and Skarland N.** Limit cycle oscillations in pacemaker cells. *IEEE Trans Biomed Eng* 47: 1134–1137, 2000.
25. **Ermentrout B.** XPP/XPPAUT [Online]. Dept. of Mathematics, University of Pittsburgh. http://www.math.pitt.edu/~bard/xpp/xpp.html [2003].
26. **Fänge R, Persson H, and Thesleff S.** Electrophysiologic and pharmacological observations on trypsin-disintegrated embryonic chick hearts cultured in vitro. *Acta Physiol Scand* 38: 173–183, 1956.
27. **Fischmeister R, Ayer RK Jr, and DeHaan RL.** Some limitations of the cell-attached patch clamp technique: a two-electrode analysis. *Pflügers Arch* 406: 73–82, 1986.
28. **Flaschberger P.** *Der Einfluß des Ca^{2+}-Agonisten BAY-K-8644 auf die Spontanaktivität embryonaler Hühnchenventrikelzellen* (Doctoral dissertation). Graz, Austria: Karl-Franzens University, 1994.
29. **Fujii S, Ayer RK Jr, and DeHaan RL.** Development of the fast sodium current in early embryonic chick heart cells. *J Membr Biol* 101: 209–223, 1988.
30. **Guan S, Lu Q, and Huang K.** A discussion about the DiFrancesco-Noble model. *J Theor Biol* 189: 27–32, 1997.
31. **Guevara MR and Jongsma HJ.** Three ways of abolishing automaticity in sinoatrial node: ionic modeling and nonlinear dynamics. *Am J Physiol Heart Circ Physiol* 262: H1268–H1286, 1992.
32. **Guevara MR and Lewis TJ.** A minimal single-channel model for the regularity of beating in the sinoatrial node. *Chaos* 5: 174–183, 1995.
33. **Guevara MR, van Ginneken ACG, and Jongsma HJ.** Patterns of activity in a reduced ionic model of a cell from the rabbit sinoatrial node. In: *Chaos in Biological Systems*, edited by Degn H, Holden AV, and Olsen LF. New York: Plenum, 1987, p. 5–12.
34. **Hagiwara N, Irisawa H, Kasanuki H, and Hosoda S.** Background current in sino-atrial node cells of the rabbit heart. *J Physiol* 448: 53–72, 1992.
35. **Hershman KM and Levitan ES.** Cell-cell contact between adult rat cardiac myocytes regulates Kv1.5 and Kv4.2 K^+ channel mRNA expression. *Am J Physiol Cell Physiol* 275: C1473–C1480, 1998.
36. **Honjo H, Boyett MR, Kodama I, and Toyama J.** Correlation between electrical activity and the size of rabbit sino-atrial node cells. *J Physiol* 496: 795–808, 1996.
37. **Hund TJ, Kucera JP, Otani NF, and Rudy Y.** Ionic charge conservation and long-term steady state in the Luo-Rudy dynamic cell model. *Biophys J* 81: 3324–3331, 2001.
38. **Jacob R, Lieberman M, and Liu S.** Electrogenic sodium-calcium exchange in cultured embryonic chick heart cells. *J Physiol* 387: 567–588, 1987.
39. **Jacob R, Lieberman M, Murphy E, and Piwnica-Worms D.** Effect of sodium-potassium pump inhibition and low sodium on membrane potential in cultured embryonic chick heart cells. *J Physiol* 387: 549–566, 1987.
40. **Josephson IR and Sperelakis N.** Tetrodotoxin differentially blocks peak and steady-state sodium channel currents in early embryonic chick ventricular myocytes. *Pflügers Arch* 414: 354–359, 1989.
41. **Josephson IR and Sperelakis N.** Developmental increases in the inwardly-rectifying K^+ current of embryonic chick ventricular myocytes. *Biochim Biophys Acta* 1052: 123–127, 1990.
42. **Kawano S and DeHaan RL.** Low-threshold current is major calcium current in chick ventricle cells. *Am J Physiol Heart Circ Physiol* 256: H1505–H1508, 1989.
43. **Kawano S and DeHaan RL.** Analysis of the T-type calcium channel in embryonic chick ventricular myocytes. *J Membr Biol* 116: 9–17, 1990.
44. **Kawano S and DeHaan RL.** Developmental changes in the calcium currents in embryonic chick ventricular myocytes. *J Membr Biol* 120: 17–28, 1991.
45. **Kneller J, Ramirez RJ, Chartier D, Courtemanche M, and Nattel S.** Time-dependent transients in an ionically based mathematical model of the canine atrial action potential. *Am J Physiol Heart Circ Physiol* 282: H1437–H1451, 2002.
46. **Kodama I, Boyett MR, Nikmaram MR, Yamamoto M, Honjo H, and Niwa R.** Regional differences in effects of E-4031 within the sinoatrial node. *Am J Physiol Heart Circ Physiol* 276: H793–H806, 1999.
47. **Kodama I, Honjo H, and Boyett MR.** Are we lost in the labyrinth of the sinoatrial node pacemaker mechanism? *J Cardiovasc Electrophysiol* 13: 1303–1305, 2002.
48. **Koidl B and Tritthart HA.** The effects of ouabain on the electrical and mechanical activities of embryonic chick heart cells in culture. *J Mol Cell Cardiol* 12: 663–673, 1980.
49. **Koidl B and Tritthart HA.** D-600 blocks spontaneous discharge, excitability and contraction of cultured embryonic chick heart cells. *J Mol Cell Cardiol* 14: 251–257, 1982.
50. **Koidl B, Tritthart HA, and Erkinger S.** Cultured embryonic chick heart cells: photometric measurement of the cell pulsation and the effects of calcium ions, electrical stimulation and temperature. *J Mol Cell Cardiol* 12: 165–178, 1980.
51. **Koidl B, Tritthart HA, and MacLeod RS.** Different effects of calcium-antagonists on automaticity in single pacemaker cells and in synchronized networks of cultured embryonic heart muscle cells. *J Mol Cell Cardiol* 18: 207–217, 1986.
52. **Kowtha VC, Kunysz A, Clay JR, Glass L, and Shrier A.** Ionic mechanisms and nonlinear dynamics of embryonic chick heart cell aggregates. *Prog Biophys Mol Biol* 61: 255–281, 1994.
53. **Krogh-Madsen T, Glass L, Doedel EJ, and Guevara MR.** Apparent discontinuities in the phase-resetting response of cardiac pacemakers. *J Theor Biol* 230: 499–519, 2004.
54. **Kurata Y, Hisatome I, Imanishi S, and Shibamoto T.** Dynamical description of sinoatrial node pacemaking: improved mathematical model for primary pacemaker cell. *Am J Physiol Heart Circ Physiol* 283: H2074–H2101, 2002.
55. **Kurata Y, Hisatome I, Imanishi S, and Shibamoto T.** Roles of L-type Ca^{2+} and delayed-rectifier K^+ currents in sinoatrial node pacemaking: insights from stability and bifurcation analyses of a mathematical model. *Am J Physiol Heart Circ Physiol* 285: H2804–H2819, 2003.
56. **Lakatta EG, Maltsev VA, Bogdanov KY, Stern MD, and Vinogradova TM.** Cyclic variation of intracellular calcium: a critical factor for cardiac pacemaker cell dominance. *Circ Res* 92: E45–E50, 2003.
57. **Le Douarin G, Renaud JF, Renaud D, and Coraboeuf E.** Influence of insulin on sensitivity to tetrodotoxin of isolated chick embryo heart cells in culture. *J Mol Cell Cardiol* 6: 523–529, 1974.
58. **Lei M, Honjo H, Kodama I, and Boyett MR.** Characterisation of the transient outward K^+ current in rabbit sinoatrial node cells. *Cardiovasc Res* 46: 433–441, 2000.
59. **Lei M, Honjo H, Kodama I, and Boyett MR.** Heterogeneous expression of the delayed-rectifier K^+ currents $i_{K,r}$ and $i_{K,s}$ in rabbit sinoatrial node cells. *J Physiol* 535: 70–74, 2001.
60. **Levitan ES, Gealy R, Trimmer JS, and Takimoto K.** Membrane depolarization inhibits Kv1.5 voltage-gated K^+ channel gene transcription and protein expression in pituitary cells. *J Biol Chem* 270: 6036–6041, 1995.
61. **Lieberman M and Paes de Carvalho A.** The spread of excitation in the embryonic chick heart. *J Gen Physiol* 49: 351–363, 1965.
62. **Liu S, Stimers JR, and Lieberman M.** Whole-cell current associated with Na-Ca exchange in cultured chick cardiac myocytes. *Ann NY Acad Sci* 639: 468–470, 1991.
63. **Liu S, Stimers JR, and Lieberman M.** A novel Cl^- conductance in cultured chick cardiac myocytes: role of intracellular Ca^{2+} and cAMP. *J Membr Biol* 141: 59–68, 1994.
64. **Liu YM, DeFelice LJ, and Mazzanti M.** Na channels that remain open throughout the cardiac action potential plateau. *Biophys J* 63: 654–662, 1992.
65. **Luo CH and Rudy Y.** A model of the ventricular cardiac action potential. Depolarization, repolarization, and their interaction. *Circ Res* 68: 1501–1526, 1991.
66. **Luo CH and Rudy Y.** A dynamic model of the cardiac ventricular action potential. I. Simulations of ionic currents and concentration changes. *Circ Res* 74: 1071–1096, 1994.
67. **Mazzanti M and DeFelice LJ.** K channel kinetics during the spontaneous heart beat in embryonic chick ventricle cells. *Biophys J* 54: 1139–1148, 1988.
68. **Mazzanti M, DeFelice LJ, and Liu YM.** Gating of L-type Ca^{2+} channels in embryonic chick ventricle cells: dependence on voltage, current and channel density. *J Physiol* 443: 307–334, 1991.
69. **McDonald TF and Sachs HG.** Electrical activity in embryonic heart cell aggregates. Developmental aspects. *Pflügers Arch* 354: 151–164, 1975.
70. **McDonald TF, Sachs HG, and DeHaan RL.** Development of sensitivity to tetrodotoxin in beating chick embryo hearts, single cells, and aggregates. *Science* 176: 1248–1250, 1972.
71. **Mitsuiye T, Shinagawa Y, and Noma A.** Sustained inward current during pacemaker depolarization in mammalian sinoatrial node cells. *Circ Res* 87: 88–91, 2000.
72. **Nathan RD and DeHaan RL.** Voltage clamp analysis of embryonic heart cell aggregates. *J Gen Physiol* 73: 175–198, 1979.

73. **Noble D, Denyer JC, Brown HF, and DiFrancesco D.** Reciprocal role of the inward currents $i_{b,Na}$ and i_f in controlling and stabilizing pacemaker frequency of rabbit sino-atrial node cells. *Proc R Soc Lond B Biol Sci* 250: 199–207, 1992.
74. **Nygren A, Fiset C, Firek L, Clark JW, Lindblad DS, Clark RB, and Giles WR.** Mathematical model of an adult atrial cell. *Circ Res* 82: 63–81, 1998.
75. **Oei HI, van Ginneken ACG, Jongsma HJ, and Bouman LN.** Mechanisms of impulse generation in isolated cells from the rabbit sinoatrial node. *J Mol Cell Cardiol* 21: 1137–1149, 1989.
76. **Ono K and Ito H.** Role of rapidly activating delayed rectifier K^+ current in sinoatrial node pacemaker activity. *Am J Physiol Heart Circ Physiol* 269: H453–H462, 1995.
77. **Pandit SV, Clark RB, Giles WR, and Demir SS.** A mathematical model of action potential heterogeneity in adult rat left ventricular myocytes. *Biophys J* 81: 3029–3051, 2001.
78. **Pappano AJ and Sperelakis N.** Low K^+ conductance and low resting potentials of isolated single cultured heart cells. *Am J Physiol* 217: 1076–1082, 1969.
79. **Pelzmann B.** *Die Wirkung von Bariumionen auf Spontanaktivität und Ionenströme isolierter embryonaler Hühnerherzventrikelzellen* (Doctoral dissertation). Graz, Austria: Karl-Franzens University, 1996.
80. **Rosati B and McKinnon D.** Regulation of ion channel expression. *Circ Res* 94: 874–883, 2004.
81. **Sachs HG, McDonald TF, and DeHaan RL.** Tetrodotoxin sensitivity of cultured embryonic heart cells depends on cell interactions. *J Cell Biol* 56: 255–258, 1973.
82. **Sada H, Ban T, Fujita T, Ebina Y, and Sperelakis N.** Developmental change in fast Na channel properties in embryonic chick ventricular heart cells. *Can J Physiol Pharmacol* 73: 1475–1484, 1995.
83. **Sada H, Ban T, Fujita T, Ebina Y, and Sperelakis N.** Role of the steady-state Na^+ channel current in pacemaker depolarizations in young embryonic chick ventricular myocytes. *Jpn J Pharmacol* 69: 159–166, 1995.
84. **Satoh H.** Identification of and developmental changes in transient outward current in embryonic chick cardiomyocytes. *Reprod Fertil Dev* 7: 1369–1374, 1995.
85. **Satoh H and Sperelakis N.** Hyperpolarization-activated inward current in embryonic chick cardiac myocytes: developmental changes and modulation by isoproterenol and carbachol. *Eur J Pharmacol* 240: 283–290, 1993.
86. **Schanne OF, Qu J, Haddad GE, and Ruiz-Petrich E.** Membrane dysfunction and abnormal spontaneous activity: a study in explanted cardiac cells. In: *Membrane Physiopathology*, edited by Bkaily G. Boston: Kluwer, 1994, p. 47–70.
87. **Shrier A and Clay JR.** Pacemaker currents in chick embryonic heart cells change with development. *Nature* 283: 670–671, 1980.
88. **Shrier A and Clay JR.** Comparison of the pacemaker properties of chick embryonic atrial and ventricular heart cells. *J Membr Biol* 69: 49–56, 1982.
89. **Shrier A and Clay JR.** Repolarization currents in embryonic chick atrial heart cell aggregates. *Biophys J* 50: 861–874, 1986.
90. **Shrier A, Clay JR, and Brochu RM.** Effects of tetrodotoxin on heart cell aggregates. Phase resetting and annihilation of activity. *Biophys J* 58: 623–629, 1990.
91. **Silva J and Rudy Y.** Mechanism of pacemaking in I_{K1}-downregulated myocytes. *Circ Res* 92: 261–263, 2003.
92. **Smith PL, Baukrowitz T, and Yellen G.** The inward rectification mechanism of the HERG cardiac potassium channel. *Nature* 379: 833–836, 1996.
93. **Spector PS, Curran ME, Zou A, Keating MT, and Sanguinetti MC.** Fast inactivation causes rectification of the I_{Kr} channel. *J Gen Physiol* 107: 611–619, 1996.
94. **Sperelakis N.** Electrical properties of embryonic heart cells. In: *Electrical Phenomena in the Heart*, edited by De Mello WC. New York: Academic, 1972, p. 1–61.
95. **Sperelakis N and Lehmkuhl D.** Insensitivity of cultured chick heart cells to autonomic agents and tetrodotoxin. *Am J Physiol* 209: 693–698, 1965.
96. **Sperelakis N and Lehmkuhl D.** Ionic interconversion of pacemaker and nonpacemaker cultured chick heart cells. *J Gen Physiol* 49: 867–895, 1966.
97. **Sperelakis N and McLean MJ.** The electrical properties of embryonic chick cardiac cells. In: *Fetal and Newborn Cardiovascular Physiology*, edited by Longo LD and Reneau DD. New York: Garland STPM, 1978, p. 191–236.
98. **Sperelakis N and Shigenobu K.** Changes in membrane properties of chick embryonic hearts during development. *J Gen Physiol* 60: 430–453, 1972.
99. **Stimers JR, Liu S, and Lieberman M.** Apparent affinity of the Na/K pump for ouabain in cultured chick cardiac myocytes. Effects of Na_i and K_o. *J Gen Physiol* 98: 815–833, 1991.
100. **Stimers JR, Shigeto N, and Lieberman M.** Na/K pump current in aggregates of cultured chick cardiac myocytes. *J Gen Physiol* 95: 61–76, 1990.
101. **Van Mierop LHS.** Location of pacemaker in chick embryo heart at the time of initiation of heartbeat. *Am J Physiol* 212: 407–415, 1967.
102. **Varghese A and Sell GR.** A conservation principle and its effect on the formulation of Na-Ca exchanger current in cardiac cells. *J Theor Biol* 189: 33–40, 1997.
103. **Varghese A and Winslow RL.** Dynamics of abnormal pacemaking activity in cardiac Purkinje-fibers. *J Theor Biol* 168: 407–420, 1994.
104. **Veldkamp MW, de Jonge B, and van Ginneken ACG.** Decreased inward rectifier current in adult rabbit ventricular myocytes maintained in primary culture: a single-channel study. *Cardiovasc Res* 42: 424–433, 1999.
105. **Veldkamp MW, Wilders R, Baartscheer A, Zegers JG, Bezzina CR, and Wilde AAM.** Contribution of sodium channel mutations to bradycardia and sinus node dysfunction in LQT3 families. *Circ Res* 92: 976–983, 2003.
106. **Verheijck EE, van Ginneken ACG, Bourier J, and Bouman LN.** Effects of delayed rectifier current blockade by E-4031 on impulse generation in single sinoatrial nodal myocytes of the rabbit. *Circ Res* 76: 607–615, 1995.
107. **Verheijck EE, van Ginneken ACG, Wilders R, and Bouman LN.** Contribution of L-type Ca^{2+} current to electrical activity in sinoatrial nodal myocytes of rabbits. *Am J Physiol Heart Circ Physiol* 276: H1064–H1077, 1999.
108. **Verheijck EE, Wilders R, Joyner RW, Golod DA, Kumar R, Jongsma HJ, Bouman LN, and van Ginneken ACG.** Pacemaker synchronization of electrically coupled rabbit sinoatrial node cells. *J Gen Physiol* 111: 95–112, 1998.
109. **Verkerk AO and van Ginneken ACG.** Considerations in studying the transient outward K^+ current in cells exhibiting the hyperpolarizing-activated current. *Cardiovasc Res* 52: 517–518, 2001.
110. **Verkerk AO, Wilders R, Coronel R, Raveslot JH, and Verheijck EE.** Ionic remodeling of sinoatrial node cells by heart failure. *Circulation* 108: 760–766, 2003.
111. **Walsh KB, Begenisich TB, and Kass RS.** β-Adrenergic modulation of cardiac ion channels. *J Gen Physiol* 93: 841–854, 1989.
112. **Wellis DP, DeFelice LJ, and Mazzanti M.** Outward sodium current in beating heart cells. *Biophys J* 57: 41–48, 1990.
113. **Wettwer E, Grundke M, and Ravens U.** Differential effects of the new class III antiarrhythmic agents almokalant, E-4031 and *d*-sotalol, and of quinidine, on delayed rectifier currents in guinea pig ventricular myocytes. *Cardiovasc Res* 26: 1145–1152, 1992.
114. **Wilders R and Jongsma HJ.** Beating irregularity of single pacemaker cells isolated from the rabbit sinoatrial node. *Biophys J* 65: 2601–2613, 1993.
115. **Wilders R, Jongsma HJ, and van Ginneken ACG.** Pacemaker activity of the rabbit sinoatrial node. A comparison of mathematical models. *Biophys J* 60: 1202–1216, 1991.
116. **Xu A and Guevara MR.** Two forms of spiral-wave reentry in an ionic model of ischemic ventricular myocardium. *Chaos* 8: 157–174, 1998.
117. **Yasui K, Liu W, Opthof T, Kada K, Lee JK, Kamiya K, and Kodama I.** I_f current and spontaneous activity in mouse embryonic ventricular myocytes. *Circ Res* 88: 536–542, 2001.
118. **Yeh BK and Hoffman BF.** The ionic basis of electrical activity in embryonic cardiac muscle. *J Gen Physiol* 52: 666–681, 1968.
119. **Zaniboni M, Pollard AE, Yang L, and Spitzer KW.** Beat-to-beat repolarization variability in ventricular myocytes and its suppression by electrical coupling. *Am J Physiol Heart Circ Physiol* 278: H677–H687, 2000.
120. **Zaza A, Micheletti M, Brioschi A, and Rocchetti M.** Ionic currents during sustained pacemaker activity in rabbit sino-atrial myocytes. *J Physiol* 505: 677–688, 1997.
121. **Zhang H, Holden AV, Kodama I, Honjo H, Lei M, Varghese T, and Boyett MR.** Mathematical models of action potentials in the periphery and center of the rabbit sinoatrial node. *Am J Physiol Heart Circ Physiol* 279: H397–H421, 2000.